C. N. R. Rao et al.

DOI: 10.1002/anie.201301548

Nanomaterials

# Graphene Analogues of Inorganic Layered Materials

*C. N. R. Rao,* H. S. S. Ramakrishna Matte, and Urmimala Maitra*

**Keywords:**
Boron nitride · graphene · layered materials · molybdenum sulfide

*Dedicated to Professor Chunli Bai on the occasion of his 60th birthday*

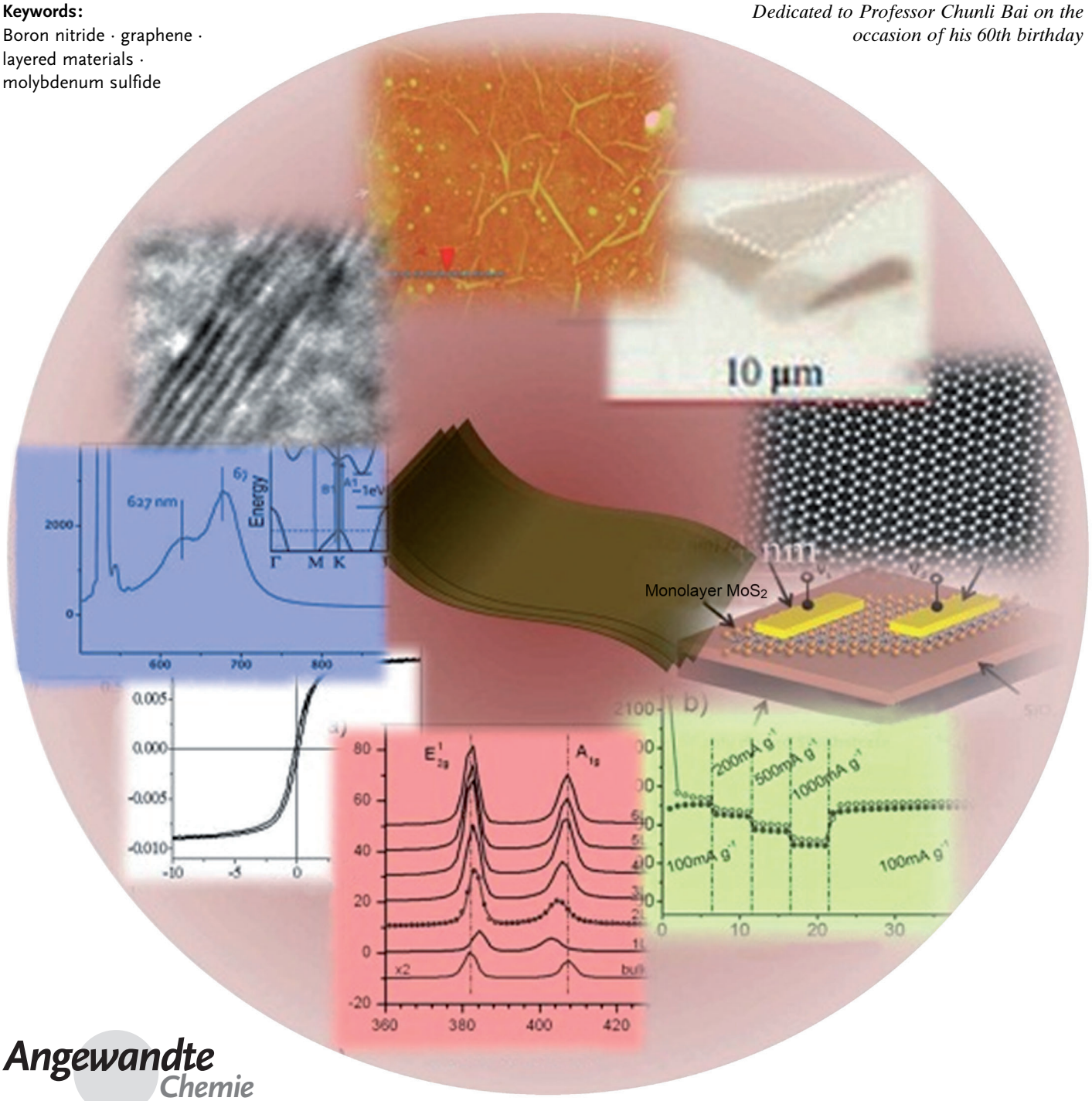

*The discovery of graphene has created a great sensation in chemistry, physics, materials science, and related areas. The unusual properties of graphene have aroused interest in other layered materials, such as molybdenum sulfide and boron nitride. In the last few years, single- as well as few-layer as well as chalcogenides and other inorganic materials have been prepared and characterized by a variety of methods. These materials possess interesting properties, and some have potential applications. This Review provides an up-to-date account of these emerging two-dimensional nanomaterials. Not only are the synthesis and characterization covered, but also important aspects such as spectroscopic and optical properties, magnetic and electrical properties, as well as applications. Salient features of the composites formed from the layered inorganic structures with graphene and polymers are presented along with a brief description of borocarbonitrides.*

**From the Contents**



## 1. Introduction

Of all the recent developments in the chemistry of materials, the discovery of graphene has created the greatest sensation because of its fascinating properties.[1] This two-dimensional network of $sp^2$ carbon atoms exhibits high electron mobility and ballistic conduction because of its unusual electronic structure. In the last six to seven years, the synthesis, properties, and applications of graphene have been pursued widely. Besides single-layer graphene, two-, three-, and other layered graphenes are being investigated. The discovery of graphene has also drawn attention to the study of other two-dimensional materials. Just as the inorganic analogues of zero-dimensional fullerenes and one-dimensional carbon nanotubes were prepared some time ago, in the last two to three years serious efforts have been made to generate graphene-like layered inorganic structures.[2] One should indeed be able to study the structure and properties of single- and few-layer structures of a wide variety of such inorganic materials. These materials exhibit interesting properties and offer much scope for study. Besides layered chalcogenides such as $MoS_2$, $WS_2$, $MoSe_2$, and $WSe_2$, there are other layered inorganic materials such as gallium selenide and boron nitride, the latter being isoelectronic with graphene. There are also layered oxides and metal–organic frameworks. It should be possible to generate single- as well as few-layer structures of oxides and metal–organic frameworks and study their layer-dependent properties.

In this Review we discuss the synthesis and characterization of some important classes of layered inorganic materials including metal chalcogenides, oxides, BN, and metal–organic frameworks. We then examine magnetic, optical, spectroscopic, and other important properties. Besides single- and few-layer structures of inorganic compounds, there have been efforts to prepare composites of the layered structures with graphene and other materials, a typical example being composites of $MoS_2$ with graphene and polyaniline, and of graphene with BN. We present salient features of such composites and review applications of the graphene analogues of layered inorganic materials in areas such as electronics, batteries, supercapacitors, catalysis, radiation detection, and gas sensing.

## 2. Synthesis and Characterization

The various methods employed for the synthesis and characterization of graphene[3] are used equally effectively in the case of the graphene analogues of inorganic layered materials.

Thus, single- and few-layer and inorganic compounds can be prepared by both physical and chemical methods. The physical methods include deposition of ultrathin films by laser ablation and sputtering, exfoliation by micromechanical cleavage (scotch-tape technique), and ultrasonication of dispersions in liquids. Micromechanical cleavage was the first successful method for generating graphene and it has been used with materials such as $MoS_2$.[2a–d] Ultrasonication has been employed universally in the case of many of the layered inorganic layered materials.[4] Layer-by-layer assembly can be used together with a judicious choice of the chemical species required for charge neutralization where

[*] Prof. Dr. C. N. R. Rao, H. S. S. Ramakrishna Matte, U. Maitra
International Centre for Materials Science
Chemistry and Physics of Materials Unit
Sheik Saqr Laboratory and CSIR Centre of Excellence in Chemistry
Jawaharlal Nehru Centre for Advanced Scientific Research
Jakkur P. O., Bangalore 560 064 (India)
E-mail: cnrrao@jncasr.ac.in

necessary. Sheets of many metal oxides are negatively charged and would require the use of an appropriate neutralizing species such as alkylammonium ions.

Chemical methods that can be employed to generate sheets of layered structures include chemical vapor deposition (CVD), atomic layer deposition (ALD), and precursor decomposition. Hydrothermal and high-temperature solid-state reactions have been employed in certain cases. Intercalation by metals and other species followed by exfoliation is a common method that is employed successfully to generate single- and few-layer inorganic structures. In particular, intercalation with an alkali metal such as lithium, followed by exfoliation in water is accompanied by the highly exothermic reaction of lithium with water, which favors exfoliation.

Single or few-layer samples of inorganic layered materials may pick up foreign atoms or molecules from the medium depending on the inherent properties of the sheets and the foreign atoms/molecules. For example, electron-donating species may adhere to the $MoS_2$ surface, while molecules with lone pairs of electrons may stick to the B sites of BN sheets.

Single- and few-layer materials are generally characterized by transmission electron microscopy (TEM) and scanning probe microscopy (SPM). Atomic force microscopy (AFM) has emerged as an essential tool to determine the number of layers or layer thickness. In favorable cases, some of the layer-dependent properties can be investigated by Raman spectroscopy. Structural characterization of the layers is carried out by a variety of spectroscopic and microscopic techniques.

### 2.1. $MoS_2$ and Related Dichalcogenides

Crystalline $MoS_2$ occurs in nature as the mineral molybdenite. Dickson and Pauling[5] took a Laue photograph of molybdenite with the incident beam normal to the basal plane and found a hexagonal axis and six symmetry planes. This structure contains two $MoS_2$ units in a hexagonal unit cell with $d(0001) = 12.30$ Å. In the 1960s, Frindt showed that micromechanical cleavage can be employed to obtain thin sheets of $MoS_2$ with thicknesses of 3.5 to 4.0 nm, which roughly corresponds to 5–6 layers.[6] In the 1980s, efforts were made to obtain single layers by using lithium intercalation. $MoS_2$ could be exfoliated into single layers by lithium intercalation followed by exfoliation in water. The absence of the {002}, {103}, and {105} reflections in the X-ray diffraction pattern is characteristic of one-molecule-thick sheets.[7] Lithium intercalation was difficult with $WS_2$ compared to $MoS_2$, and was achieved through intercalation of *n*-butyllithium through sonication for long periods in hexane.[8] The intercalation time does not significantly increase the Li concentration, but increases as the intercalation temperature increases, with saturation attained when the temperature reaches 100 °C.[9a] As early as 1986, Koma and Yoshimura[9b] obtained defect-free single-layer $MoS_2$ and $MoSe_2$ by van der Walls epitaxy. Frindt and co-workers[10] carried out a detailed structural investigation of single-layer $MoS_2$ by X-ray diffraction and found that Mo atoms are coordinated in an octahedral manner in contrast to the trigonal prismatic coordination in bulk $MoS_2$. These results were supported by Raman spectroscopy and energy X-ray absorption fine-structure analysis.

Micromechanical exfoliation, which is found to be effective in generating single layers of graphene, can also be employed in the case of $MoS_2$. Ultrasonication, which is another simple procedure for the synthesis of defect-free graphene dispersions from bulk graphite, has been employed to obtain single and multiple layers of transition-metal dichalcogenides such as $MoS_2$, $WS_2$, $MoSe_2$, $MoTe_2$, $TaSe_2$, $NbSe_2$, and $NiTe_2$.[4] BN and $Bi_2Te_3$ can also be exfoliated in organic solvents through sonication. The concentrations of the resulting $MoS_2$ and $WS_2$ suspensions are 0.30 and 0.15 mg mL$^{-1}$, respectively. The important factor when choosing the appropriate solvent for any given material is that the solvent and the material should have similar surface energy. Such material suspensions can blend with solutions of other nanomaterials or polymers, thereby giving rise to composites for various applications.[4] A detailed study of $MoS_2$ carried out by the same research group reports the importance of sonication time and centrifuge speed for obtaining the maximum concentration of $MoS_2$. The dispersed concentration can be increased to about 40 mg mL$^{-1}$ by increasing the sonication time to 200 h. However, the lateral size of the flake was found to be approximately 700 nm after 60 h, after which it falls off because of scission. After centrifuging the dispersion at 5000 rpm, the flakes had a mean length and width of $\langle l \rangle \approx 0.3$ μm and $\langle w \rangle \approx 0.15$ μm, whereas dimensions

*C. N. R. Rao obtained his PhD from Purdue University (1958) and DSc from the University of Mysore (1961). He is the National Research Professor and Linus Pauling Research Professor at the Jawaharlal Nehru Centre for Advanced Scientific Research, Honorary Professor at the Indian Institute of Science (both at Bangalore), and a member of many science academies. His awards include the Einstein Gold Medal of UNESCO, the Hughes and Royal Medals of the Royal Society, the August Wilhelm von Hofmann medal of the German Chemical Society, the Dan David Prize, the Illy Trieste Science prize for materials research, and the first India Science Prize.*

*H. S. S. Ramakrishna Matte obtained his BSc from Government College, Rajahmundry in 2006 and MS and PhD in chemical science in 2009 and 2013, respectively, from the Jawaharlal Nehru Centre for Advanced Scientific Research, working on nanomaterials.*

of the flake generated at 300 rpm increased to $\langle l \rangle \approx 2\,\mu m$ and $\langle w \rangle \approx 1.2\,\mu m$.[11] Zhou et al.[12] reported a mixed-solvent strategy for exfoliating inorganic layered materials that was based on Hansen solubility parameters and found that ethanol/water at an appropriate ratio gives $0.018\,mg\,mL^{-1}$ for $MoS_2$ and $0.032\,mg\,mL^{-1}$ for $WS_2$. Later, Yao et al.[13] reported a procedure involving the use of low-energy ball milling combined with sonication for the exfoliation of inorganic layered materials, with $1.2\,mg\,mL^{-1}$ for BN and $0.8\,mg\,mL^{-1}$ for $MoS_2$ in 0.05 wt% sodium dodecylsulfate (SDS)/water.

The lithium intercalation procedure has been revisited and the chalcogenide product characterized with various microscopy techniques. A typical lithium-intercalation reaction is essentially done in two steps. The first step involves intercalation of the layered material with lithium by soaking 100 mg of $MoS_2/WS_2/MoSe_2/WSe_2$ in 10 mL *n*-butyllithium in 5 mL hexane for 72 h at 373 K in a nitrogen atmosphere. The intercalated samples are washed with hexane several times to remove any remaining *n*-butyllithium. For exfoliation, water is added, during which a profuse evolution of gas occurs, thereby giving rise to an opaque suspension of single- and few-layer $MoS_2/WS_2/MoSe_2/WSe_2$.[14] The synthesis of nanosheets of layered materials such as $MoS_2$, $WS_2$, $TiS_2$, $TaS_2$, and $ZrS_2$ have been reported by intercalating lithium electrochemically and subsequent exfoliation in water.[15] Few-layer-thick BN, $NbSe_2$, $WSe_2$, $Sb_2Se_3$, and $Bi_2Te_3$ nanosheets have also been synthesized from the bulk counterparts by electrochemical lithium intercalation in which the cut-off voltage and discharge current were optimized.[16]

Another important method for the synthesis of few-layer graphene analogues of sulfides and selenides of molybdenum on a large scale involves the use of thiourea/selenourea as the sulfur and the selenium sources, respectively. In a typical synthesis, molybdic acid/tungstic acid is ground with thiourea/selenourea (1:48 ratio), placed in an alumina boat, and heated to 773 K inside a horizontal tube furnace for 3 h in a $N_2$ atmosphere to obtain few-layer $MoS_2$ $WS_2$, $MoSe_2$, and $WSe_2$.[14] This method essentially produces single- to few-layer graphene analogues. Figure 1 shows the characterization of chemically synthesized graphene analogues of a few-layer chalcogenide.

Large-area $MoS_2$ thin layers are prepared by high-temperature annealing of a thermally decomposed ammonium thiomolybdate layer in the presence of sulfur.[17] Chemical vapor deposition on $SiO_2/Si$ substrates has been used to synthesize $MoS_2$ layers by using $MoO_3$ and S powders as reactants. The growth of $MoS_2$ layers is promoted by coating the substrate with graphene oxide and potassium perylene-3,4,9,10-tetracarboxylate.[18] Recently, few-layer $MoS_2$ was synthesized on a graphitic surface by heating amorphous $MoS_3$ and reduced graphite oxide at 1000 °C under high-vacuum conditions.[19]

Large-area $MoS_2$ films were grown on a $SiO_2$ substrate by predeposition of a Mo film by using elemental sulfur as the sulfur source under chemical vapor deposition conditions at temperatures of 500–750 °C.[20] Single-layer $MoS_2$ is obtained on a sulfur-preloaded copper surface, where the sulfur source is only available to generate the first $MoS_2$ monolayer.[21] Wafer-scale $MoS_2$ thin layers can be synthesized by using $MoO_3$ thin films as the starting material, followed by a two-step thermal process, reduction of $MoO_3$ at 500 °C in hydrogen, and sulfurization at 1000 °C by using sulfur on the *c*-face

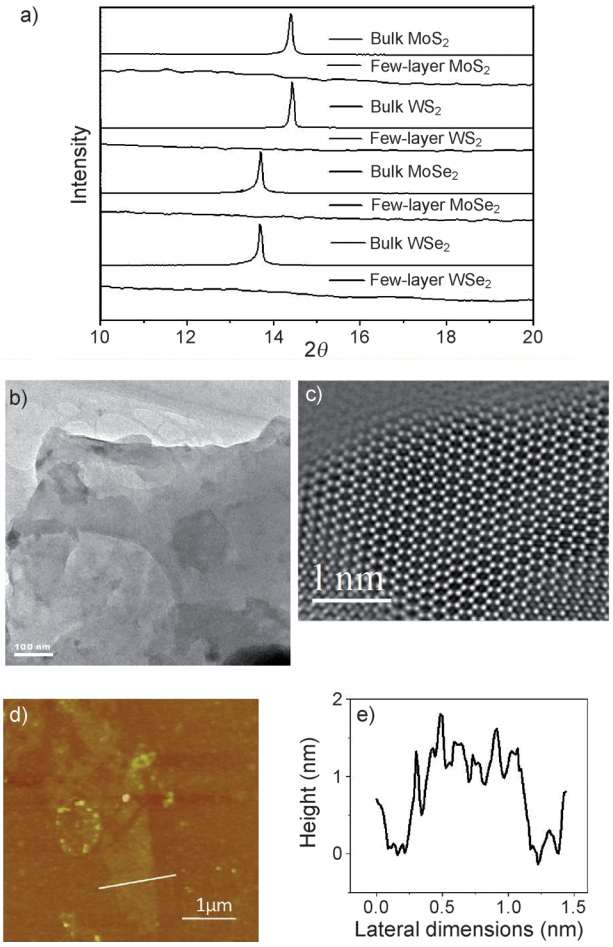


***Figure 1.*** a) XRD patterns of bulk samples and few-layer $MoS_2$, $WS_2$, $MoSe_2$, and $WSe_2$ obtained by the thiourea/selenourea method. b) TEM image of few-layer $WSe_2$ obtained by Li intercalation. Scale bar: 100 nm. c) HREM image of single-layer $MoSe_2$ obtained by the selenourea method. d) AFM image of few-layer $MoSe_2$ obtained by Li intercalation. e) The corresponding height profile. (Adapted from Ref. [14].)

*Urmimala Maitra obtained her BSc from Banaras Hindu University in 2007 and MS in Materials Science in 2010 from Jawaharlal Nehru Centre for Advanced Scientific Research. She is currently carrying out PhD studies on inorganic graphene analogues and other nanomaterials.*

of a sapphire substrate. These layers are easily transferred on to various substrates.[22]

Hydrothermal synthesis has been used to prepare few-layer graphene analogues of $MoS_2$ and $MoSe_2$. Few-layer $MoS_2$ is obtained starting from $MoO_3$ and KSCN (as the sulfur source) and water as the solvent at 453 K. $MoSe_2$ layers were prepared by using a molybdic acid and selenium metal with $NaBH_4$ as the reducing agent at 453 K.[14] The same precursors have been used to obtain few-layer $MoS_2$ and $MoSe_2$ under microwave conditions by using ethylene glycol as the solvent. The precursors are placed in a teflon-coated autoclave, heated at 450 W for 15 min and 20 min, respectively, in a domestic microwave oven operating at 2.45 GHz to yield graphene analogues of $MoS_2$ and $MoSe_2$.[23] Free-standing nanosheets of $MoS_2$ and $WS_2$ can also be synthesized by low-temperature (360 °C) decomposition of single-source precursors (ammonium tetrathiotungstate, ammonium tetrathiomolybdate) in oleylamine.[24]

Laser-thinning of multilayered $MoS_2$ provides a reliable approach to obtain single-layer $MoS_2$ with a defined shape and size. The semiconducting properties of laser-fabricated single-layer $MoS_2$ are comparable to those of pristine single-layer $MoS_2$ (see Figure 2a–c).[25] Laser-irradiation of dispersions of bulk metal dichalcogenides ($MoS_2$/$WS_2$/$MoSe_2$ and $WSe_2$) in dimethylformamide by a KrF excimer laser, with a laser fluence of 1.5 J cm$^{-2}$ and a repetition rate of 5 Hz for 1 h, has been used to produce single- and few-layer materials. After laser exfoliation, the resultant solutions are kept for 24 h and then centrifuged at 2500 rpm for 5 min. Figure 2d shows a TEM image of few-layer $MoS_2$ obtained by laser exfoliation. Figure 2e and f show a topographic AFM image and the corresponding height profile of exfoliated $MoS_2$ with a thickness of about 1 nm and lateral dimensions of a few hundred nanometers.[23]

### 2.2. Other Layered Chalcogenides

Mechanical exfoliation has been the principle method for generating large-area single-layer sheets of several-layered transition-metal sulfides. Gacem et al.[26] have developed a technique based on anodic bonding to exfoliate a variety of layered materials. Various materials exfoliated by this method include $MoS_2$, $NbSe_2$, GaSe, GaS, InSe, $Bi_2Sr_2CaCu_2O_x$, $CuGeO_3$, $TiS_2$, and mica. Colloidal nanosheets of several Group IV and Group V transition-metal sulfides and selenides have been prepared from metal chlorides and $CS_2$ or metallic Se by heating them to high temperatures in oleylamine. 2D layered structures of $TiS_2$, $ZrS_2$, $HfS_2$, $VS_2$, $NbS_2$, and $TaS_2$ as well as $TiSe_2$, $ZrSe_3$, $HfSe_3$, $VSe_2$, $NbSe_2$, and $TaSe_2$ with thicknesses of around 30 nm and lateral dimensions of around 250 nm have been obtained.[27] The approach provides a general method for the synthesis of a large number of 2D layered materials, but the thickness of the synthesized nanosheets is quite large.

Atomically thin sheets of GaS and GaSe have been deposited on $SiO_2$/Si substrates and characterized by optical microscopy, AFM, and Raman spectroscopy.[28] Figure 3a–f shows optical microscopic and AFM images and the corresponding height profiles of GaS nanosheets with a thickness of around 1 nm obtained by micromechanical cleavage. Optical microscopy provides a convenient way to determine the number of layers. Optical contrast varies with the thickness of $SiO_2$ on the Si. The transistor action and photodetection properties of these materials have been studied.[29] Heating GaS and GaSe powders in sealed quartz tubes leads to the deposition of sheets of GaS and GaSe.[30] Diphenyldiselenide has been used as a precursor for the synthesis of GaSe.[31] Single-crystalline CdS nanosheets can be prepared by vapor deposition and show a 1D nanobelt to 2D nanosheet transformation.[32]

Nanosheets of $VS_2$ were prepared from bulk $VS_2$ by swelling and intercalation by sonication in formamide. These nanosheets were used to prepare flexible moisture-sensing devices for touchless positioning.[33] $VS_2$ nanosheets can also be obtained by sonication of a precursor formed under hydrothermal conditions from sodium orthovanadate and thioacetamide.[34] Ultrathin sheets of $Co_9Se_8$ were synthesized hydrothermally from cobalt acetate and $SeO_2$. The material shows interesting magnetic properties.[35] Single- and few-layer $TaS_2$ and $TaSe_2$ on Si/$SiO_2$ were prepared by Li et al.[36] and characterized by Raman microscopy.

Vapor-phase deposition is used to deposit GeS nanosheets on a Si-(100) substrate under low pressure (20–40 Torr) and low temperature (300 °C). Boundary layer diffusion

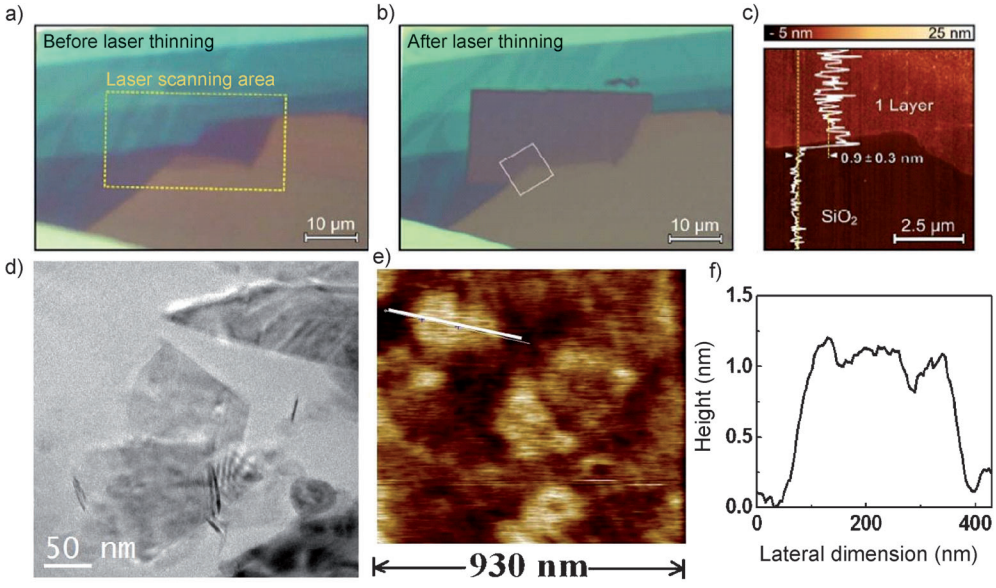


*Figure 2.* a) Optical microscopy image of a multilayered $MoS_2$ flake deposited onto a 285 nm $SiO_2$/Si substrate. b) Same as in (a) after scanning a laser in the area marked by a dashed rectangle in (a). c) Topographic AFM images of the region marked by the square in (b). A vertical topographic line profile is included in (c) to indicate the thickness of the laser-thinned layer. d) TEM and e) AFM images as well as f) height profile for laser-exfoliated MoS2 sheets in DMF. (Adapted from Refs. [23] and [25].)

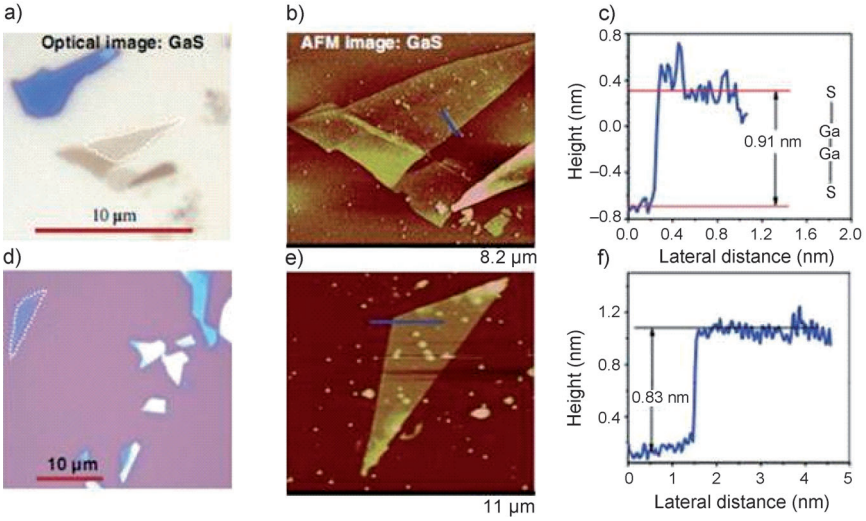


***Figure 3.*** Optical images of ultrathin GaS flakes (shown by dashed line) deposited on a) 50 nm and d) 300 nm $SiO_2$/Si. b,e) AFM images and c,e) height profile for the structures shown in (a) and (d), respectively. (Adapted from Ref. [29].)

is proposed to be the rate-determining step in the growth process.[37] GeS nanosheets of 3–20 nm thickness have been prepared from $GeI_4$ and hexamethyldisilazane in oleylamine.[38] Large-area single-crystalline SnS nanosheets are obtained by the thermal decomposition of the single-source precursor (tin-diethyldithiocarbamate-1,10-phenanthroline).[39] Free-standing nanosheets of SnSe can be prepared from $SnCl_2$ and trioctylphosphineselenide (TOPSe) and hexamethyldisilazane in oleylamine.[40] The thickness of the sheets can be tuned (10–40 nm) by adjusting the concentrations of $SnCl_2$ and TOPSe. Zhai et al.[41] carried out the hydrothermal synthesis of nanosheets of $SnS_2$ from tin(IV) chloride and thioacetamide. The nanosheets show a reversible capacity and good cycling stability for use in Li-ion batteries. Hydrothermal treatment of a tin foil with cysteine yields vertically aligned nanosheets of $SnS_2$, with a high capacity of 1050 $mAh\,g^{-1}$ and a good photocatalytic activity for the degradation of dyes.[42] PbS nanosheets of around 50 nm thickness prepared under hydrothermal conditions with cysteine as the sulfur source and ethylenediamine as the growth inducer have exposed (100) facets.[43]

Heating thioacetamide and $InCl_3$ in hexadecyltrimethylammonium bromide (CTAB) at reflux yields $In_2S_3$ nanosheets with high reversible capacity in Li-ion batteries.[4] $In_2S_3$ nanosheets can also be prepared by heating indium diethyldithiocarbamate trihydrate (In-DDTC) in octadecylamine and hexadecylamine solution to 200 °C.[44] The nanosheets were doped with Cu and their photoresponse studied. Single-crystalline nanosheets of $Sb_2Te_3$ are obtained from $SbCl_3$, $Na_2TeO_3$, and hydrazine hydrate in ethylene glycol under microwave heating.[2c] The reaction of $SbCl_3$ and $TeO_2$ with hydrazine hydrate as the reducing agent and polyvinyl alcohol as the surfactant under hydrothermal conditions yields $Sb_2Te_3$ nanobelts and nanosheets. The nanobelts slowly transform into nanosheets with longer reaction times.[45]

Nanodiscs of $Bi_2Se_3$ are prepared by heating $Bi(NO_3)_3$ and $Na_2SeO_3$ in the presence of different surfactants in ethylene glycol and a small amount of $NH_2OH$. The morphology of the discs depends on the surfactant and the temperature of the reaction mixture. Amine-containing surfactants enlarge the lateral dimensions of the discs and yield ultrathin nanosheets.[46] Atomically thin layers of $Bi_2Te_3$ are obtained by mechanical cleavage. Quintuple building blocks (i.e. five monoatomic sheets of Te(1)-Bi-Te(2)-Bi-Te(1)) of 1 nm thickness were most prevalent, while further cleavage sometimes yielded just a few atomic planes.[47] $Bi_2Te_3$ nanosheets could also be prepared on Si substrates from a physical mixture of Bi and Te by surface-assisted chemical vapor transport. The sheets had a thickness of less than 3 nm, which corresponds to one or two quintiples of $Bi_2Te_3$. A TEM image of a nanosheet of $Bi_2Te_3$ is shown in Figure 4a. Figure 4b shows the Raman spectra of the as-prepared $Bi_2Te_3$ nanosheets at different spots and show two kinds of spectra with higher and lower signal intensities.[48] The Raman signal becomes stronger as the thickness of the $Bi_2Te_3$ sheets decreases. Simple vapor-phase deposition by heating $Bi_2Te_3$ and $Bi_2Se_3$ in an Ar atmosphere yields nanoplates on $SiO_2$/Si substrates.[49] First principles calcula-

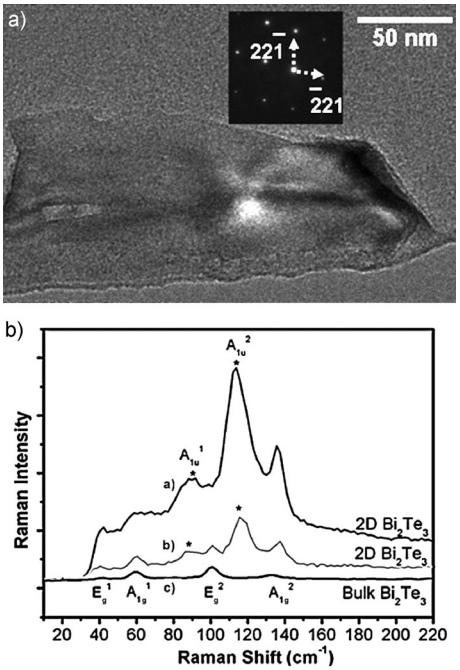


***Figure 4.*** a) Low-magnification TEM image of a $Bi_2Te_3$ nanosheet. The inset is the corresponding SAED pattern viewed down the (1012) direction. b) Raman spectra of $Bi_2Te_3$ nanosheets (from two different areas of the same sample and bulk $Bi_2Te_3$. Adapted from Ref. [48].)

  

tions have been employed to predict several new layered materials that can be stabilized in single-layer hexagonal honeycomb lattices.[50] Alloys of several metal chalcogenides such as $MoS_2/MoSe_2/MoTe_2$ have been shown to be thermodynamically stable at room temperature.[51] Wen et al.[52] proposed a two-dimensional CdSe structure with wave (buckled) and flat (graphene-type) structures, with the isolated CdSe sheet being effectively flat. Theoretical calculations predict intriguing properties for some of these layered materials. For example, vacancy-doped or nonmetal-adsorbed monolayers of sufides, selenides, and tellurides of Mo and W are proposed to show long-range antiferromagnetic coupling.[53] Similarly, pristine single-layers of $VS_2$ and $VSe_2$ are predicted to be magnetic, and tunable through the application of strain.[54]

### 2.3. Boron Nitride

Boron nitride is the structural analogue of graphene, with a hexagonal unit consisting of 3 B and 3 N atoms. BN is, however, an insulator and its layers could find uses as dielectric gates and so on.[55] A monolayer BN film was first prepared by the pyrolysis of borazine on single-crystalline Ni and Cu substrates.[56] Corso et al.[57] observed that a nanomesh-like morphology is obtained a on Rh(111) substrate with a high lattice mismatch. The use of a different chemical precursor such as trichloroborazine instead of borazine leads to the formation of BN islands and superstructures.[58]

Free-standing few-layer BN flakes can be obtained by micromechanical cleavage.[59] Few-layer BN flakes obtained by mechanical cleavage can be thinned down to monolayers by reactive ion etching[60] or by irradiation with a high-energy electron beam.[61] Ball milling has also been used to prepare BN nanosheets.[62] The method, however, yields BN sheets with a high density of defects. BN nanosheets can be exfoliated by applying a shear force on the surface of bulk BN. Chen et al.[63] rotated a dispersion of BN in NMP (*N*-methyl-2-pyrrolidone) at 8000 rpm at an angle of 45° in a vortex fluidic device to exfoliate BN into nanosheets. Similar effects were obtained by application of high pressure to a dispersion of BN in a DMF/chloroform mixture flowing through a microfluidic channel.[64]

Like all layered materials, interlayer van der Waals forces in BN can be overcome by ultrasonication in solution.[65] Vigorous sonication of BN particles in a highly polar solvent such as DMF results in exfoliation.[65b] The resulting dispersion when centrifuged yields few-layer BN in the supernatant. The majority of the sheets obtained are around 10 layers thick, with the thinnest sheet having 3 layers. Polar solvents such as NMP, *N*,*N*-dimethylacetamide, and ethylene glycol can be used for the solvent-based exfoliation of BN.[55] Lin et al.[65c] carried out an exfoliation induced by chemical functionalization to obtain stable and optically transparent dispersions of few-layer BN. The amine groups of lipophilic and hydrophilic amine molecules have been used to functionalize BN nanosheets by using Lewis acid–base interactions between the amine group of the functional molecules and the electron-deficient boron atoms in BN. Interestingly, nanosheets and nanoribbons of BN could be prepared by sonication of BN in water. Water acts as a hydrolyzing agent, cutting the BN nanosheets with the release of $NH_3$.[66] Exfoliation and dispersion through noncovalent interaction was demonstrated by Han et al.[67] by using a solution of a conjugated polymer, poly(*m*-phenylenevinylene-*co*-2,5-dictoxy-*p*-phenylenevinylene) in dichloroethane.

Micromechanical cleavage and ultrasonication generally gives low yields of BN nanosheets. High yields are obtained by the combustion of boric acid with sodamide, ammonium bromide, and ammonium carbonate, followed by heating to temperatures above 1000 °C.[68] The surface segregation method, that is, vacuum thermal treatment of B- and N-doped transition-metal alloys, has long been used to prepare thin films of BN.[69] The presence of a low percentage of sulfur impurities in a Fe-Cr-Ni alloy allows the formation of predominantly mono- and bilayer BN films by surface segregation.[70] Large-area BN films are made possible by chemical-vapor deposition (CVD) of ammonia and borane or borazine on polycrystalline Ni and Cu.[71] Films as thin as 3–5 layers and a flake size of up to a few nanometers were obtained on preannealed Cu foils with ammonia-borane ($NH_3$-$BH_3$) at 1000 °C.[71a] Figure 5 shows the optical image as well as TEM and AFM images of BN films. A decaborane/ammonia mixture can also be used to prepare nanosheets of BN on polycrystalline substrates.[72] The films thus obtained need to be transferred to other substrates for characterization. The process thus involves multiple steps before the product can actually be put into application. Single- and few-layer BN films can be directly deposited on Si substrates by microwave plasma chemical-vapor deposition of $BF_3$-$H_2$-$N_2$, without the use of any catalyst.[73] The growth of BN sheets in the absence of a catalyst is ascribed to etching by the fluorine-containing gases. BN films have been grown over graphene by CVD of ammonia-borane.[74] The method has been used to prepare BN films on pyrolytic graphite or mechanically

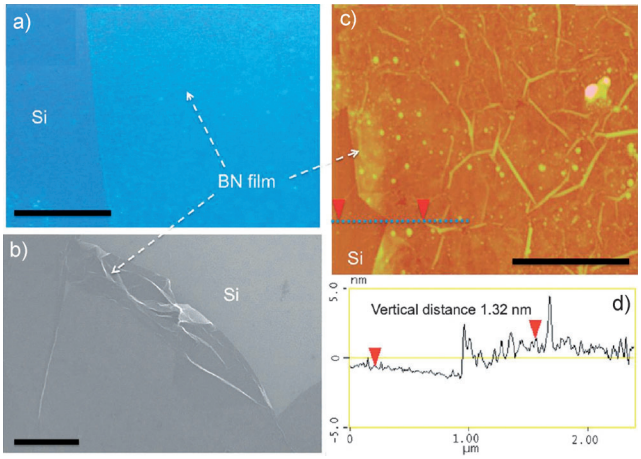


***Figure 5.*** Topography of ultrathin hexagonal BN films. a) Photograph of a large h-BN film on a silicon substrate. Scale bar: 1 cm. b) SEM image of a h-BN film (scale bar: 10 µm). c,d) AFM image and line-scan profile indicate that the h-BN film has a uniform thickness of a 1 nm. Scale bar: 2 µm. (Adapted from Ref. [71a].)

exfoliated graphene as well as stacks of graphene/BN. Graphene can be used as a sacrificial template to obtain BN and BN-C films from $B_2O_3$ and a graphene mixture treated at 1650 °C.[75] Han et al.[75] used graphene as a sacrificial template with $B_2O_3$ as the B source and $N_2$ gas as the N source to prepare BN nanosheets by heating to 1650 °C. Pakdel et al.[76] mixed boron powder with MgO and FeO catalysts to obtain vertically aligned BN nanosheets on $Si/SiO_2$ substrates.

The bulk-scale synthesis of BN nanosheets has been achieved by the reaction of boric acid with urea.[77] The method not only gives a high yield of BN sheets but also good control over the number of layers. Boric acid and urea with different molar ratios (1:6, 1:12, 1:24, and 1:48) are used to prepare BN with a different number of layers. The reactions involved in the synthesis are:

$$2\,B(OH)_3 \xrightarrow{\Delta} B_2O_3 + 3\,H_2O$$

$$NH_2CONH_2 \xrightarrow{\Delta} NH_3 + HNCO$$

$$B_2O_3 + 2\,NH_3 \xrightarrow{\Delta} 2\,BN + 3\,H_2O$$

XRD studies of the samples reveal an increase in the width of the reflections along with an increase in the *d* spacing of the (002) reflection on increasing the urea content in the precursor, thus implying a lower sheet to sheet registry. TEM images and AFM studies show samples with 8–14, 4–6, and 1–2 layers for those prepared with boric acid and urea molar ratios of 1:12, 1:24, and 1:48, respectively. A TEM image of a sample prepared with a 1:24 ratio of boric acid/urea is shown in Figure 6a. An AFM image of BN prepared with a boric acid/urea molar ratio of 1:48 is shown in Figure 6c. The height profile shows a steplike increase from 0.4 to 0.8 nm, thus indicating a single layer (Figure 6d). TEM studies show the B–N bond to be 1.44 Å and the distance between two nearest boron atoms to be 2.49 Å (Figure 6b). The BN nanosheets prepared by the urea route are readily solubilized in Lewis bases.[77] Chemical blowing is another approach for the synthesis of large volumes of single- and few-layer BN nanosheets with lateral dimensions of about 100 nm. Stepwise heating of ammonoborane results in bubble formation because of the release of hydrogen gas, such that the atomically thin walls of polymeric B-N-H collapse on annealing to form BN nanosheets.[78] High-quality two atomic layer thick BN films were grown by magnetron sputtering of boron in a mixture of $N_2$-Ar. The films showed pinhole-free insulating behavior on the $\mu m^2$ scale, thus demonstrating that they could be used as high-quality thin-film dielectrics.[79]

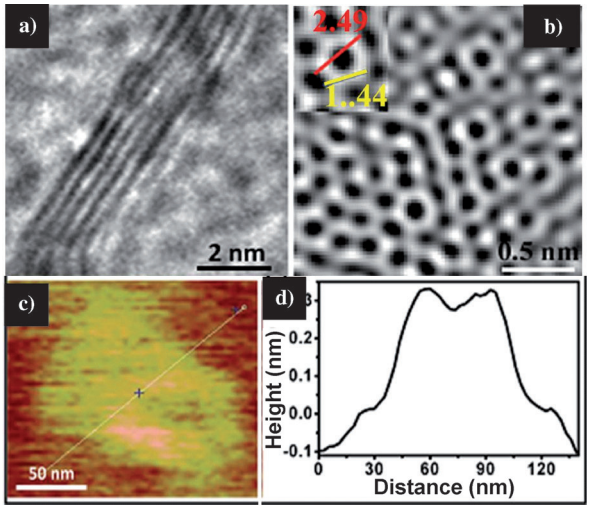


***Figure 6.*** a) TEM image of BN sheets prepared by thermal decomposition of boric acid and urea. b) High-resolution TEM image showing nearest neighbor B–N (yellow) and B–B (red) bond lengths. c) AFM image of the sample and d) the corresponding height profile. (Adapted from Ref. [77].)

### *2.4. Metal Oxides*

Two-dimensional layers or sheets of metal oxides are of importance by virtue of their properties having practical importance. Thus, the dielectric properties of single- or few-layer metal oxides have attracted considerable attention.[80] Several single-layered oxides have been prepared in recent years. These include oxides of Mn, Mo, W, Ru, Ti, and Nb (Table 1).

***Table 1:*** Some oxides, whose layers have been isolated.

| | |
|---|---|
| copper oxide | $Bi_2CaSr_2Cu_2O_x$ |
| cobalt oxide | $CoO_2^-$ |
| manganese oxide | $MnO_2$, $Mn_{1-x}M_xO_2$ (M = transition metal) |
| titanium oxide | $TiO_2$ and $Ti_{1-x}M_xO_2$ (M = transition metal) |
| niobium oxide | $Nb_3O_8$ |
| ruthenium oxide | $RuO_{2+x}$ |
| tungsten oxide | $Cs_4W_{11}O_{36}^{2-}$ |
| perovskite oxide | $Ca_2Nb_3O_{10}$, $SrTa_2O_7$, $LaNb_2O_7$, $Bi_2SrTa_2O_9$ |

In this context, the early report of the preparation of single layers of titanates by delamination of layered titanates by Sasaki and Watanabe[81] deserves special mention. An important strategy employed for delamination or exfoliation is to use intercalants such as tetrabutylammonium ions or long-chain amines. Most of the layered oxides reported have metals in the $d^0$ configuration. Of these, the dielectric properties of $TiO_2$ (or specifically $Ti_{0.87}O_2$) sheets have been investigated in detail because of their high dielectric constant, especially in the rutile structure, with the value being in the range of 80 to 100.

There are many layered perovskite oxides with interesting dielectric and other properties. Of these, oxides belonging to the Aurivillius family with the general formula $(Bi_2O_2)$ $(A_{m-1}B_mO_{3m+1})$ and the Ruddlesdon–Popper family with the general formula $A_{m+1}M_mO_{3m+1}$ are of importance. Many members of the Aurivillius family possess interesting dielectric (ferroelectric) properties, as exemplified by $Bi_4Ti_3O_{12}$. Besides the dielectric properties of the Sr-Ti-O members of the Ruddlesdon–Popper family (e.g. $Sr_3Ti_2O_7$, $Sr_4Ti_3O_{10}$), novel electronic and magnetic properties are exhibited by oxides of transition metals with a $d^n$ electronic configuration crystallizing in these structures. Sometime ago, the variation of the electronic and magnetic properties of manganese

oxides of this family with dimensionality was reported.[82] Nickel oxides of the type $Ln_{m+1}Ni_mO_{3m+1}$ (Ln = rare earth metal) exhibit different electronic properties when $m$ or the dimensionality are changed. Some members of the Dion–Jacobson family with the general formula $A'(A_{m-1}B_mO_{m+1})$ also show useful dielectric properties. Examples are found in the recent literature where nanosheets of perovskite oxides such as $Ca_2Nb_3O_{10}$ or $LaNb_2O_7$ have been used as building blocks in devices. Figure 7 shows the structures and AFM images of two-dimensional sheets of the perovskite oxides[83] $LaNb_2O_7$ and $(Ca,Sr)_2Nb_3O_{10}$. Osada and Sasaki have reviewed the dielectric properties of structures containing oxide layers.[80]

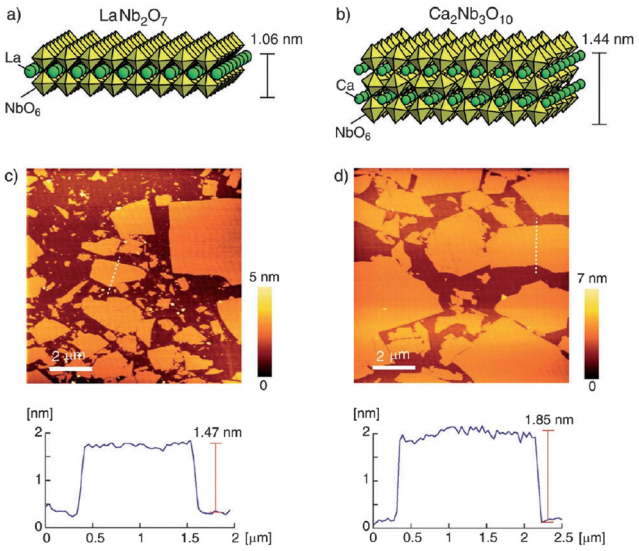


***Figure 7.*** Structures and AFM images (10×10 μm²) of a,c) $LaNb_2O_7$ and b,d) $Ca_2Nb_3O_{10}$ nanosheets. Tapping-mode AFM under vacuum condition was used to evaluate the morphology of the nanosheets on the Si substrate. Height profiles are shown in the bottom panels. (Adapted from Ref. [83].)

The variation of the dielectric constant with an increase in the number of layers is a valuable feature for the fabrication of devices. Similarly, layer-dependent magnetic properties could be of use in spintronics and other applications. There is a need to investigate the layer-dependent properties of ferro- and ferrimagnetic oxides. The use of $SnO_2$ and $TiO_2$ nanosheets in lithium batteries has been reported.[84] The sensitivity of tin oxide sensors for CO is found to increase as the number of layers decreases.[85] Layered metal hydroxides can be exfoliated by using intercalation and other chemical strategies,[86] and these materials provide a means of generating oxide layers with novel properties.

There are many studies to be done on single- and few-layer structures of metal oxides, since oxides constitute the richest class of materials with a wide range of properties. Thus, layered oxide superconductors as exemplified by bismuth cuprates could be investigated. The layer-dependent properties of layered rare-earth manganites could be investigated in regard to their magnetic and electrical properties. The single-layered structures of simple oxides such as $MoO_3$ could also be studied, since our study of few-layer $MoO_3$ prepared by different methods has revealed layer-dependent catalytic activity as well as other properties.[87] The TEM and AFM images of few-layer $MoO_3$ prepared by a chemical method are shown in Figure 8.

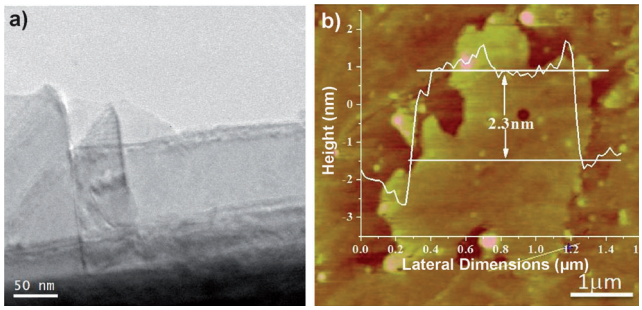


***Figure 8.*** a) TEM and b) AFM image and height profile of few-layer $MoO_3$. (Adapted from Ref. [87].)

### 2.5. Metal–Organic Frameworks

A variety of metal–organic framework (MOF) structures have been synthesized and characterized in recent years.[88] These materials based on phosphates, phosphonates, carboxylates, and sulfates can be one-, two-, or three-dimensional structures. The layered two-dimensional structures are of interest in the present context. When the layers of these materials are not held together by charged species or other species bound to an adjacent layer, the layer can in principle be exfoliated by mechanical, ultrasonic, or chemical means. Single- or few-layer metal–organic frameworks prepared in this manner have been reported recently. Nanosheets of zinc MOFs have been obtained by ultrasonication and characterized by microscopic techniques as well as Tyndall scattering.[89]

It would be worthwhile studying the magnetic properties of layered MOFs with varying layer thickness. Preliminary studies on single- and few-layer species derived from two-dimensional cobalt and nickel phosphates and carboxylates yielded interesting results. Canted antiferromagnetism and such magnetic interactions exhibited by these materials are found to be irradicated when the layer thickness becomes small. Figure 9 shows the results obtained on layered cobalt phospahate. The few-layer structures obtained by ultrasonication exhibit the Tyndal cone while the magnetic transition found in the bulk material disappears.[90]

## 3. Raman Spectroscopy

Raman spectroscopy is an essential tool for probing the structure and electronic properties of graphene. It is also used to determine the number of layers in graphene samples. As the properties of layered materials mainly depend on the number of layers, it is necessary to have a nondestructive technique to determine the thickness.[91] Resonance Raman scattering is a sensitive probe for materials that have different electronic band structures depending on the number of layers.

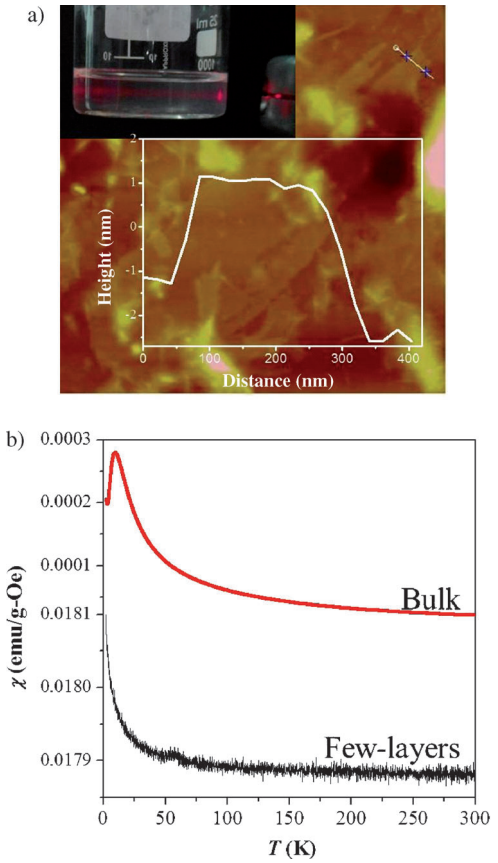


***Figure 9.*** a) AFM image of ultrasonicated layered cobalt phosphate [$Co(C_{10}H_{13}PO_3).H_2O$]. Inset: the Tyndall cone. b) Comparison of the magnetic properties of bulk (red curve) and few-layered (black curve) samples under a field of 100 Oe. (Adapted from Ref. [90].)

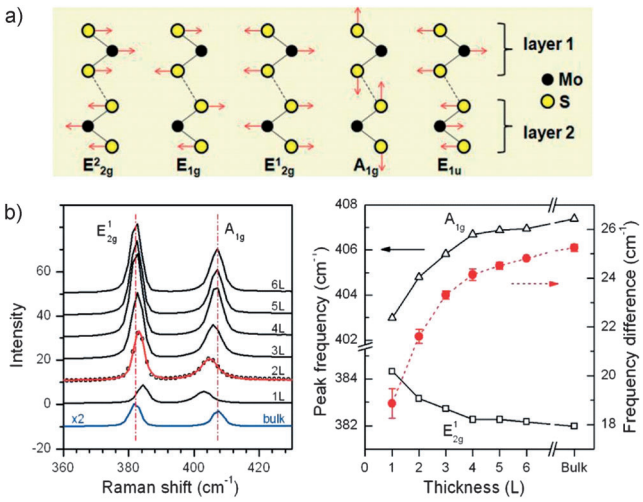


***Figure 10.*** a) The atomic displacements of the four first order Raman active modes $E^2_{2g}$, $E_{1g}$, $E^1_{2g}$, and $A_{1g}$ and one IR active mode $E_{1u}$. b) Raman spectra of thin (*n*L) and bulk $MoS_2$ films. The solid line for the 2L spectrum is a double Voigt fit through data (circles for 2L, solid lines for the rest). c) Frequencies of $E^1_g$ and $A_{1g}$ Raman modes (left vertical axis) and their difference (right vertical axis) as a function of layer thickness. (Adapted from Refs. [92] and [93].)

Group theory predicts four first-order Raman active modes for a crystal of $MoS_2$: $E^2_g$, $E_{1g}$, $E^1_g$, and $A_{1g}$ with frequencies of 32 $cm^{-1}$, 286 $cm^{-1}$, 383 $cm^{-1}$, and 408 $cm^{-1}$, respectively (Figure 10a).[92]

The $E^2_g$ mode is an interlayer mode arising from the vibration of two rigid layers against each other. All the other modes are caused by intralayer S-Mo-S atomic vibrations, among which $A_{1g}$ is the out-of-plane vibration mode and the rest are in-plane vibration modes.

The $E_{1g}$ mode is forbidden in a back-scattering geometry on the surface perpendicular to the *c*-axis. Lee et al.[93] studied the layer-dependent Raman spectra of $MoS_2$ by using a 514.5 nm laser, which corresponds to an off-resonance condition (Figure 10b). As the number of layers (*n*) decreases, the $E^1_g$ mode shows a blue shift of about 2 $cm^{-1}$ while the $A_{1g}$ mode is red-shifted by about 4 $cm^{-1}$ (Figure 10c). The line width of the $A_{1g}$ mode shows a maximum at $n = 2$, whereas the line width of the $E^1_g$ mode does not depend on *n*. A large frequency shift of the shear mode to higher wave numbers is found as the number of layers increases.[94]

Ultrathin $MoS_2$ flakes have been investigated systematically by using Raman and resonance Raman spectroscopy. The resonance Raman spectra show that the coupling between the electronic transitions and phonons becomes weaker in ultrathin $MoS_2$ compared to the bulk. This is explained on the basis of increased transition energy at the K point because of the perpendicular quantum confinement or elongated intralayer atomic bonds in ultrathin $MoS_2$. The consistent frequencies of the $E^1_g$ and $A_{1g}$ bands of monolayer $MoS_2$ on using various laser lines show that Raman spectroscopy is a reliable tool for determining the thickness of few-layer $MoS_2$.[95] Najmaei et al.[96] have studied the thermal effects on the Raman spectra of few-layer $MoS_2$ and found that there is a red-shift in the peak positions of both the $E^1_g$ and $A_{1g}$ modes as well as an increase in the line width as the laser energy increases.

Theoretical calculations have been carried out to understand the anomalous phonon behavior of few-layer $MoS_2$. Going from single-layer $MoS_2$ to bulk, we expect an increase in the frequency of the $A_{1g}$ mode because of the increase in the force constant of the extra layer. The $E_{2g}$ mode should behave similarly, but the observed stiffening can be understood on the basis of a variation of the lattice parameters. The lateral lattice constant of 3D $MoS_2$ is 3.16 Å, while for 2D $MoS_2$ it is 3.14 Å. By using these lattice parameters it was found that the frequency of the $E_{2g}$ mode increases from 381.2 to 385 $cm^{-1}$, thus confirming the anomalous effect.[97] The dependence of the $E^1_g$ mode frequency on *n* is also explained in terms of the Columbic interaction between the Mo atoms, which decreases as the number of layers increases because of the increase in the dielectric screening. This reduces the total restoring force acting on the atoms along the direction perpendicular to the plane, thereby softening the frequency with increasing *n*.[98]

The layer-dependent resonance Raman spectra of $MoS_2$ have been investigated in detail. A Raman mode at 179 $cm^{-1}$ is assigned to the two-phonon dispersion difference mode $A_{1g}(M)$-LA(M). This mode does not show any dependence on *n*. A prominent first order acoustic mode is also observed for

  

few-layer samples at 230 $cm^{-1}$, thereby indicating the presence of structural-defect-induced scattering. A mode denoted as "c" at about 377 $cm^{-1}$ can be resolved from the $E^1_g$ mode. This band is broad in the spectrum of a single layer, but becomes sharp when $n=2$, 4, and 7. The frequency of this mode does not depend on $n$. However, its relative integrated intensity with respect to the $E^1_g$ mode decreases with increasing $n$. A band appears at about 409 $cm^{-1}$ in the resonance Raman spectra, and evolves with layer thickness. It is assigned to the $B_{1u}$ mode in bulk $MoS_2$.[99] It is the Davydov couple of the $A_{1g}$ mode.[100] The intensity of this mode relative to that of the $A_{1g}$ mode increases as $n$ increases. Two second-order modes in the region 430–490 $cm^{-1}$ assigned to 2LA(M) and $A_{2u}$ show layer dependence and stiffen as $n$ increases. The relative intensity of the 2LA(M) mode with respect to the $A_{2u}$ mode also increases as $n$ increases. Three new bands are seen in the higher wavenumber region in few-layer samples (554 $cm^{-1}$ (labeled as Q), 588 $cm^{-1}$ (P), and 628 $cm^{-1}$ (S)) which are not observed in the bulk sample. The frequencies of these modes do not vary with $n$, but their relative intensities depend on $n$. The resonance Raman spectra of $MoS_2$ can thus be a handy tool for identifying the number of layers (Figure 11).[101]

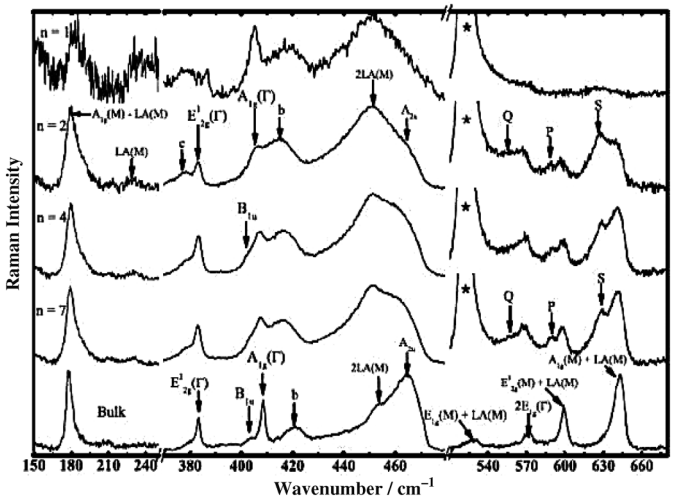


***Figure 11.*** Resonant Raman spectra of different layers of $MoS_2$ with a 633 nm laser line. The layer numbers ($n$) are marked. Different modes are marked with arrows. The strong Raman mode marked * comes from the $SiO_2$/Si substrate and is completely absent in the spectrum of thick multilayer (labeled as bulk) $MoS_2$. The symmetry assignments are also shown for different modes. The noticeable feature is the appearance of completely new modes and their evolution with layer thickness. (Adapted from Ref. [101].)

Figure 12a shows the Raman spectrum of GaSe with varying layer thickness. Figure 12b shows the Raman spectra of a 1 nm ultrathin GaSe sheet with that of a bulk GaSe crystal. In the 1 nm layer of GaSe, the Raman signals from the $A^1_g$ and $E^1_g$ modes disappear and the $E^2_g$ mode becomes more intense. The $A^2_g$ mode appears to be softened. Figure 12c,d show the effect of the layer thickness on the $A^2_g$ and $A^1_g$ bands, respectively.[28]

## 4. Optical and Related Properties

Bulk $MoS_2$ is a narrow indirect band-gap semiconductor of about 1.2 eV.[102] Density functional theory shows that a transition from an indirect band gap (Γ–K) to a direct band gap of 1.8 eV occurs at the K point for single-layer $MoS_2$ (Figure 13a).[103] The photoluminescence (PL) and reflection spectra of ultrathin layers of mechanically exfoliated $MoS_2$ reveal two bands at 1.85 eV (670 nm) and 1.98 eV (627 nm).[103a] These bands correspond to A1 and B1 excitonic transitions at the K point which arise from spin–orbit splitting of the valance band (Figure 13b,c).[103a,104] PL emissions corresponding to A1 and B1 excitonic transitions of single-layer $MoS_2$ show a huge enhancement compared to that of the bulk as a result of indirect to direct crossover. The direct band gap emission, being symmetrically allowed, is greatly enhanced compared to indirect emission, which is a weak phonon-assisted process.[103a] Such an enhancement becomes dramatic in free-standing single-layer $MoS_2$ (the quantum efficiency is about $10^4$ times that of the bulk material).[103b] Mak et al.[103b] have observed by using PL and photoconductivity measurements a progressive evolution of the direct band gap emission around 1.9 eV from the indirect gap at about 1.29 eV as the number of layers is reduced down to a single layer. Free-standing single-layer $MoS_2$ shows a PL band corresponding to only the A1 excitonic transition, while double-layer and few-layer samples show bands for both the A1 and B1 transitions. The spin-up and spin-down valence bands are thus degenerate in single-layer $MoS_2$. The presence of an underlying substrate or layer raises the degeneracy and splits the valence band, thereby giving rise to two emission bands for double- and few-layer samples as well as for single-layer samples on substrates. Photoconductivity spectroscopy of the samples shows a sudden increase in the photoconductivity at 1.8 eV, thus supporting the indirect to direct crossover. A weak emission at an energy corresponding to the indirect band gap (Γ–K) is seen in double-layer and few-layer samples, with the band position shifting to lower energies as the number of layers increases and approaches the bulk value (1.6 eV in a double layer to 1.29 eV in bulk material). The valence band maxima at the Γ point progressively shifts towards the K point on decreasing the number of layers.

Chemical exfoliation of $MoS_2$ by Li intercalation results in the loss of the pristine semiconducting properties of the sample along with the loss of the PL emission, a consequence of the transition to a metastable metallic 1T state from the stable semiconducting 2H state. The absorption spectra show a gradual emergence and enhancement in the characteristics of the $MoS_2$ bands with increasing annealing temperature up to 300 °C. The increase in film thickness results in a slight red-shift of both the absorption and photoluminescence bands. Weak interlayer coupling between the restacked layers is a possible reason for the gradual decrease in the emission.[105]

Zhao et al.[106] have studied the absorption and photoluminescence properties of mechanically exfoliated $WS_2$ and $WSe_2$ with various number of layers ($n=1$, 2,…5; Figure 14a,b). Excitonic absorption bands appear at 625 and 550 nm for $WS_2$ and at 760 and 600 nm for $WSe_2$, with all the bands exhibiting gradual blue-shifts as the flake thickness

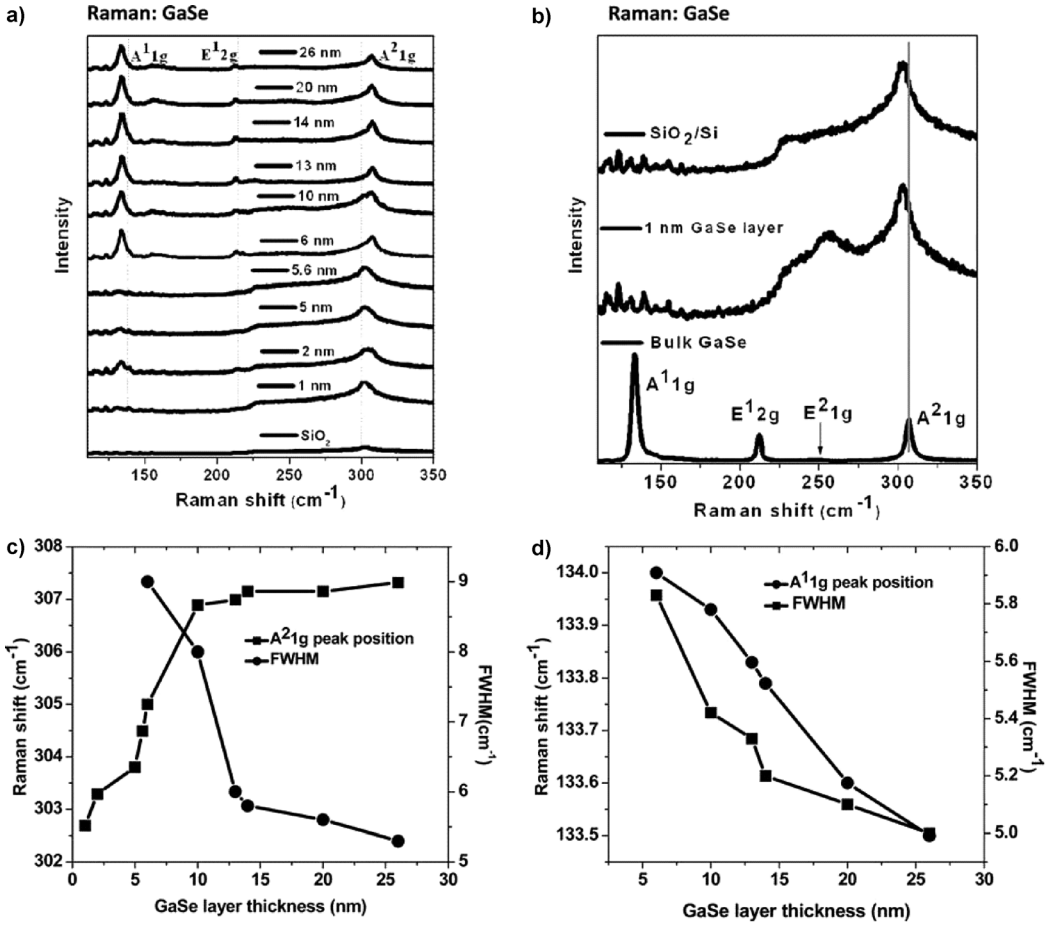


***Figure 12.*** a) Raman spectroscopy of GaSe as a function of layer thickness. The Raman spectrum of the $SiO_2$/Si substrate is also shown for reference. b) Raman spectra of $SiO_2$/Si substrate, 1 nm thick GaSe layer, and bulk GaSe. Effect of the layer thickness on the Raman modes c) $A^2_g$ and d) $A^1_g$. (Adapted from ref. [28].)

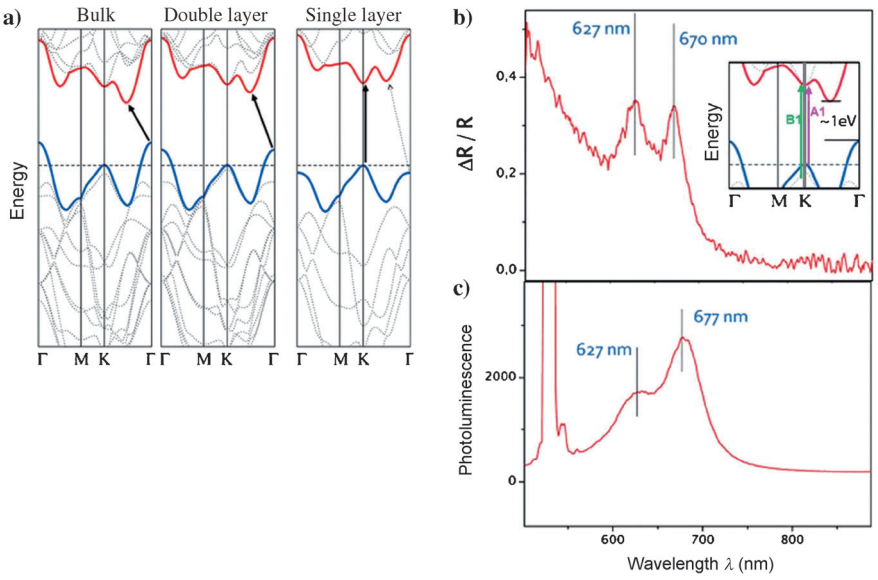


***Figure 13.*** Electronic band structure of a) bulk, double-layered and single-layered $MoS_2$. b) Reflection and c) photoluminiscence spectra of ultrathin $MoS_2$. The inset in (b) shows the simplified band structure of bulk $MoS_2$ with the A1 and B1 transitions. (Adapted from Ref. [103a].)

decreases. Additional bands appear for $WS_2$ at 450 nm and several additional peaks for $WSe_2$ in the absorption spectra. The PL emissions of single-layer samples are so strong that they can be readily distinguished from double layers under a fluorescence confocal microscope. Figure 14c,d shows the optical and confocal images of the mechanically exfoliated $WS_2$ layers. The PL emissions of single and double layers of $WS_2$ and $WSe_2$ prepared by chemical-vapor transport have greater PL quantum yields than monolayers of natural $MoS_2$.

Band-gap tuning in transition-metal chalcogenides is possible with an electric field. The indirect band gap of double-layer transition-metal chalcogenides can be driven to zero by application of electric fields of 2–3 $V\,nm^{-1}$ perpendicular to the layers, thus allowing a larger tunability of the

  

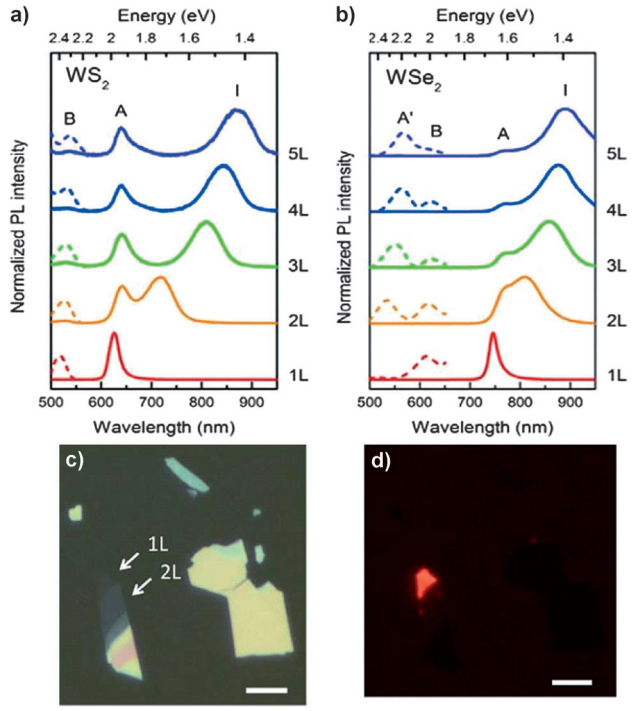


***Figure 14.*** Normalized photoluminescence spectra of mechanically exfoliated a) 2H-$WS_2$ and b) 2H-$WSe_2$ flakes for $n = 1,2,...5$. The hot electron peaks (A′ and B) are magnified as dashed lines. c) Bright-field optical image and d) corresponding fluorescence images of mechanically exfoliated $WS_2$. Scale bar: 5 μm. (Adapted from Ref. [106].)

band gap than in graphene.[107] The application of stress also allows the band gap in layered transition-metal sulfides and selenides to be tuned. First principles calculations predict that the energy gap of single- and double-layer $MoS_2$ decreases with increasing bilayer strain such that the material undergoes a metal to insulator transition at a threshold strain (tensile strain of about 18% or a compressive strain of 15%).[108] On the other hand, Yun et al.[109] employed the linearized augmented plane wave (FLAPW) method and showed that the tensile strain reduces the gap energy, while compressive strain increases it. Bhattacharya and Singh[110] showed that chalcogenides of both Mo and W undergo semiconductor to metal transition on application of a certain threshold pressure, which decreases as the chalcogen group changes from S to Te and is higher for $WX_2$ than $MoX_2$. Few-layer $MoS_2$ interacts with the electron donor tetrathiafulvalene (TTF) but not with the electron acceptor tetracyanoethylene (TCNE), with the $MoS_2$ accepting one electron from TTF and thereby forming the TTF radical cation.[111] This is understandable since $MoS_2$ is a p-type material and would not accept holes. First principles calculations show a large decrease in the band gap of $MoS_2$ on interaction with TTF.

## 5. Magnetic Properties

The observation that graphene exhibits room-temperature ferromagnetism has led to the investigation of the layer-dependent magnetism in transition-metal dichalcogenides, which have essentially the same structural features. Ferromagnetic and antiferromagnetic domains appear to coexist in graphene. This has aroused curiosity regarding the exchange bias effect in these materials, which is a phenomenon that should occur if such domains exist.

Panich et al.[112] reported that electron paramagnetic resonance (EPR) investigations of inorganic fullerene-like $MoS_2$ nanoparticles indicated the presence of a larger density of dangling bonds carrying unpaired electrons, thus indicating a more defective structure compared to the bulk sample. $MoS_2$ and $WS_2$ clusters ($Mo_6S_{12}$ and $W_6S_{12}$) have been shown to be magnetic, with the magnetism arising from the unsaturated metal center with partially filled d orbitals.[113] Zhang et al.[114] prepared $MoS_2$ with a high density of prismatic edges and showed them to be ferromagnetic at room temperature, with the magnetism arising from the nonstoichiometry of the unsaturated Mo and S atoms at the edges. Commercially available bulk $MoS_2$ was lithiated by soaking it in butyllithium in an argon atmosphere, and the Li-$MoS_2$ so obtained showed room-temperature ferromagnetism.[115] The existence of ferromagnetism in $MoS_2$ samples is attributed partly to the presence of zigzag edges in the magnetic ground state.[116] $MoS_2$ exhibits room-temperature magnetic ordering when exposed to a 2 MeV proton beam. The temperature dependence of the magnetization shows a ferromagnetic behavior with a Curie temperature of 895 K. The possible causes of the room-temperature ferromagnetism are isolated vacancies, vacancy clusters, formation of edge states, and reconstructions of the lattice.[117] Density functional calculations on $MoS_2$ layers reveal that edge states are magnetic.[118] It appears that magnetism originates at the sulfur-terminated edges because of the splitting of metallic edge states at the Fermi level.

The magnetic properties of graphene-like sulfides and selenides of Mo and W have been reported. Figure 15a shows temperature-dependent magnetization data of a few-layered $MoSe_2$ sample at 500 Oe. The divergence between the field-cooled (FC) and zero-field-cooled (ZFC) data starts around 300 K. This type of behavior is observed in magnetically frustrated systems such as spin glasses, where ferromagnetic and antiferromagnetic domains are distributed randomly. Anomalies are observed at around 50–80 K, which are similar to that of graphene, thus confirming the presence of ferromagnetic and antiferromagnetic domains.[119] Figure 15b shows the room-temperature hysteresis of few-layer $MoSe_2$. Figure 15c shows the exchange bias behavior in few-layer $MoS_2$ samples under different fields. A negative exchange bias of 15.5 Oe is observed with an applied field of 1 T. The exchange bias decreases as the applied field decreases, and reverses to −15.5 O on application of a bias field of −1 T (Figure 15d).

First-principles calculations on arm-chair $MoS_2$ have shown that it has a spin-unpolarized ground state, whereas zigzag $MoS_2$ nanoribbons are in the spin-polarized state. It is argued that zigzag $MoS_2$ nanoribbons with a ribbon width on the nanoscale will be magnetic.[120] Atomically resolved HREM images of single-layer $MoS_2$ and $MoSe_2$ show the presence of zigzag edges. Raman spectroscopy can also be used to characterize defect-related bands in few-layer

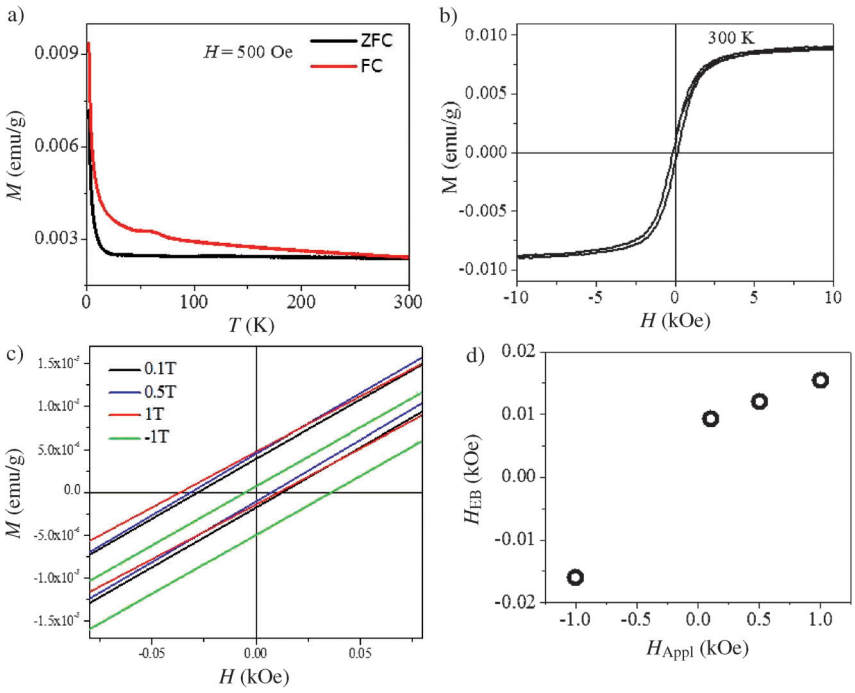


***Figure 15.*** a) Temperature-dependent magnetization (zero-field cooled (ZFC) and field-cooled (FC)) of few-layer $MoSe_2$ under 500 Oe field. b) Hysteresis of few-layer $MoSe_2$ at 300 K. c) Plot of magnetization versus field of few-layer $MoS_2$ at 2 K cooled under different applied fields. d) Dependence of exchange bias on the applied field. (Adapted from Ref. [119].)

$MoSe_2$.[1d] In addition to the $E^1_g$ and $A_{1g}$ modes which are characteristics of $MoS_2$, the appearance of the 450 $cm^{-1}$ mode as a result of second-order LA(M) phonons indicates the presence of defects.[121] It is noteworthy that defect-related magnetism is observed in nanoparticles of inorganic nanomaterials, such as ZnO and $Al_2O_3$, which are otherwise nonmagnetic. The observation of magnetism in $MoS_2$ and other dichalcogenides may be useful in certain applications.[122]

## 6. Superconducting Properties

There is considerable interest in the possibility of two-dimensional superconductivity occurring in layer compounds. Taniguchi et al.[123] have recently reported the superconducting properties of $MoS_2$ with a critical temperature ($T_c$) of 9.4 K. In $NbSe_2$, each layer consists of a sheet of Nb atoms between two sheets of Se atoms, with the separation between the sheets being 6.3 Å. Bulk $NbSe_2$ is a superconductor with a $T_c$ value of 8.3 K. Frindt[124] pointed out that the superconducting transition temperature changes with the thickness of the $NbSe_2$ slabs. There were subsequent efforts to synthesize various structures of $NbSe_2$,[125] but there is no report yet on the superconducting properties of graphene-like structures synthesized by chemical methods.

Few-layer $NbSe_2$ has been synthesized by grinding 1 mM niobium powder with 2 mM selenium granules for 20 min to uniformity and the tube was flame-sealed under a vacuum of 10–5 torr. It was placed in a vertically aligned tube furnace and heated to 1000 °C over 8 h, maintained at that temperature for 2 h, then cooled to 800 °C over 2 h, and kept at 800 °C for 4 days. Finally, the system was allowed to cool to room temperature over 10 h. Figure 16a shows the XRD patterns of the bulk and few-layer $NbSe_2$ samples. Figure 16b shows the HREM image of $NbSe_2$ with the hexagonal arrangement of niobium and selenium atoms. The AFM image in Figure 16c confirms the presence of two layers with a height of 1.6 nm and lateral dimensions in the range 200–500 nm. Magnetic measurements carried out with a Squid magnetometer at 20 Oe on bulk and the few-layer samples show a decrease in the $T_c$ value in the few-layer material (Figure 16d). On careful examination, it can be seen that the transition starts around 6.5 K and shows a break at 3.6 K. This behavior would be expected if the sample were a mixture of single- and few-layer $NbSe_2$, with the 3.6 K transition arising from the single layer.[126a] The lower $T_C$ value of few-layer $NbSe_2$ suggests that electron–phonon coupling and the electron density of states at the Fermi level changes significantly in the few-layer sample, thereby causing a decrease in the $T_C$ value.[126]

Hybrids of layered materials with other organic and inorganic materials can be used to obtain new and otherwise unrealized properties. Coronado et al.[127] obtained materials with superconducting and single-molecular magnetic properties by engineering $Mn_4$ clusters between superconducting $TaS_2$ sheets.

## 7. Field-Effect Transistors

The main advantage of graphene-based field-effect transistors (FETs) is the associated high carrier mobility of up to $10^6$ $cm^2 Vs^{-1}$.[128] Several problems remain with graphene because of the absence of a band gap, which is essential for transistor applications. Considerable effort has been made to open the band gap of graphene by reducing its dimensions, so as to form graphene nanoribbons.[65a] In this context, there has been an extensive search for other layered materials that are analogous to graphene and possess semiconducting characteristics.[129] Novoselov et al.[129] fabricated a FET on single-layer $MoS_2$ prepared by mechanical exfoliation by back-gate device fabrication. The mobilities are reported to be in the range 0.5–3 $cm^2 Vs^{-1}$. Radisavljevic et al.[130] modified the fabrication procedure by using $HfO_2$ as the top gate dielectric. At room temperature, single-layer $MoS_2$ FETs have mobilities of about 200 $cm^2 Vs^{-1}$, with current on/off ratios of $10^8$:1 and ultralow standby power dissipation.

A detailed study has been carried out on back-gated FETs based on single-layer $MoS_2$ to understand the hysteresis in these transistors. It appears to be primarily due to large

  

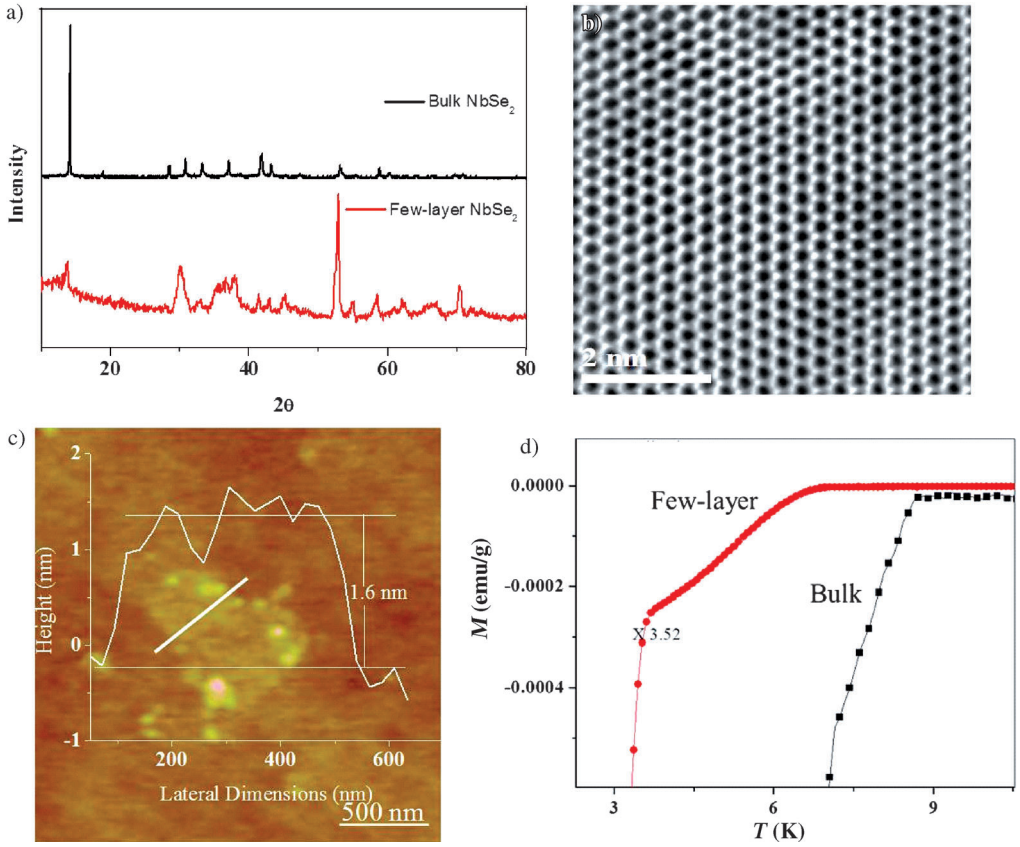


***Figure 16.*** a) XRD patterns of the bulk samples of $NbSe_2$ and few-layer $NbSe_2$. b) HREM images of $NbSe_2$. c) AFM image and the associated height profile of $NbSe_2$. d) Temperature-dependent magnetization of bulk $NbSe_2$ and few-layer $NbSe_2$ at $H = 20$ Oe. For comparison with the bulk data, data for few-layer $NbSe_2$ multiplied by 3.52 is shown. (Adapted from Ref. [126a].)

trapping states induced by absorbed water molecules on the $MoS_2$ surface and also because of the photosensitivity of $MoS_2$ devices. $MoS_2$ devices have been fabricated by using electron beam lithography and electron beam evaporation of Ti (5 nm)/Au (150 nm) (see Figure 17a). Figure 17b shows how the hysteresis steadily increases with relative humidity (RH) from 4 V (12% RH, black curve) to 15 V (22% RH, blue curve) to 25 V (60% RH, red curve), with the current at $V_{gs} = 37$ V decreasing continuously. This might be due to a higher density of trapping states induced by the increasing humidity. Figure 17c shows the hysteresis characteristic of the device under dark and light conditions. In the dark mode, the threshold voltage moves to the positive side in both sweeping directions. The hysteresis is dramatically

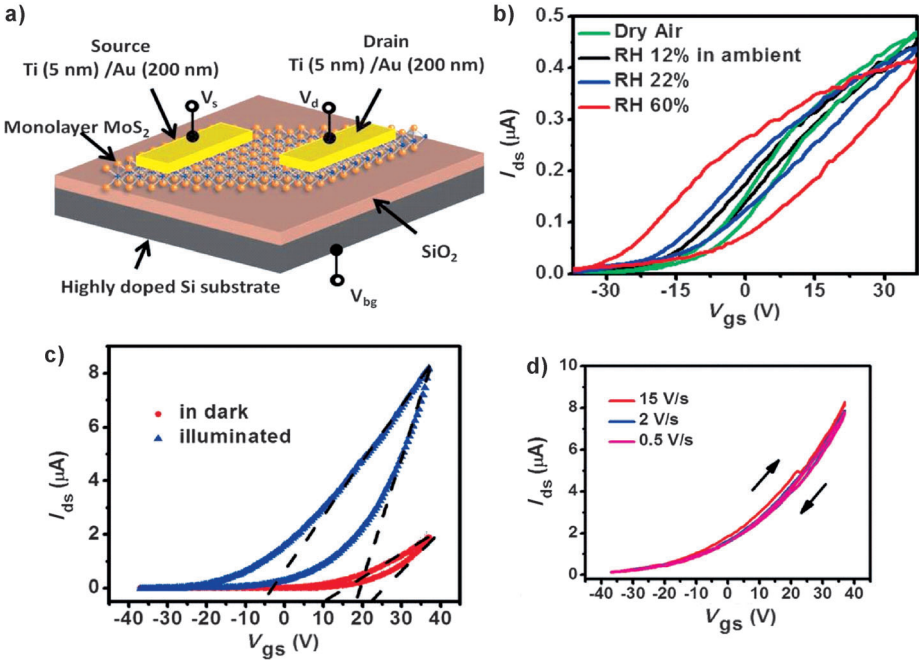


***Figure 17.*** a) Schematic representation of single-layer $MoS_2$ FET with highly doped silicon as the back gate. b) Hysteresis evolution of the same device under different humidity. c) Hysteresis in a single-layer $MoS_2$ transistor with different illumination conditions. Blue dots are under global illumination with white light (0.7 mW cm$^{-2}$), and red dots are in the dark. d) The hysteresis behavior of $I_{ds}$–$V_{gs}$ is almost removed even at a slow scan rate such as 0.5 V s$^{-1}$. (Adapted from Ref. [131].)

decreased under illumination with white light, as the change of threshold voltage in the hysteresis goes further down to 10 V from 20 V. Uniform encapsulation of the device has been carried out with silicon nitride to minimize the hysteresis. The conductivity of the transistor increases by over 100 times after passivation with a 30 nm thick $Si_3N_4$ layer. It becomes nearly hysteresis-free at various gate-bias sweeping rates and the mobility is enhanced by over one order of magnitude from 1.7 to 71.8 $cm^2 Vs^{-1}$, probably because of the improved contact and suppressed Coulomb scattering (Figure 17 d).[131]

Transistors have been fabricated with single-layer $MoS_2$ and with $Al_2O_3$ used as a top-gate dielectric. Capacitance–voltage measurements reveal that there is a good interface between the single-layer $MoS_2$ and $Al_2O_3$. The field-effect mobility of electrons when using the top gate is 517 $cm^2 Vs^{-1}$ with high current on/off ratios over $10^8$:1.[132] Min et al.[133] studied the effect of nanosheet thickness on the performance of a $MoS_2$ FET with an $Al_2O_3$ top gate. The mobility of single-layer $MoS_2$ is found to be 170 $cm^2 Vs^{-1}$ with a subthreshold swing (SS) of 90 mV $dec^{-1}$, whereas double- and triple-layer FETs show mobilities of 25 and 15 $cm^2 Vs^{-1}$ with SS values of 0.5 and 1.1 V $dec^{-1}$, respectively. This decrease in the performance of the devices is attributed to the increase in the dielectric constant with increasing thickness. A transistor fabricated on a 15 nm thick $MoS_2$ sheet obtained by mechanically exfoliation of $MoS_2$ has demonstrated that it has ambipolar characteristics. It has an on/off ratio of over 200:1. Hall effect measurements show that the hole mobility (86 $cm^2 Vs^{-1}$) is larger than that of the electrons (44 $cm^2 Vs^{-1}$), thus suggesting that a p-type operation is more favorable in FET devices.[134] $MoS_2$ thin-film transistors fabricated with ion gel gate dielectrics have shown a low threshold voltage ($<1$ V), high mobility (12.5 $cm^2 Vs^{-1}$), and a high on/off current ratio ($10^5$:1). These transistors exhibit high mechanical flexibility and no degradation in their electrical characteristics.[135] Chakraborthy et al.[136] reported an carrier-dependent in situ Raman study of a top-gated single-layer $MoS_2$ transistor with on-off ratio of about $10^5$:1 and a mobility of 50 $cm^2 Vs^{-1}$. It is shown that the $A_{1g}$ phonon mode softens and broadens with electron doping, whereas the $E_{2g}$ mode remains inert up to an electron doping of $2 \times 10^{13}$ $cm^2$.

Lee et al.[137] reported the fabrication of a two-terminal device and FET based on $MoS_2$ prepared by liquid-phase exfoliation. They found n-type FET characteristics with small on/off ratios of 3:1–4:1 and mobilities of 0.117 $cm^2 Vs^{-1}$. The possible reasons for the low mobilities may be the adsorption of solvent remnants or impurities that come from the exfoliation procedure. Low-temperature electrical transport measurements in FET devices with one, two, and three layers of $MoS_2$ have shown that electrons are localized up to room temperature at most gate voltages and display variable range hopping transport as the temperature is lowered. The disorder likely arises from the Coulomb potential of randomly distributed charges at the $MoS_2$–$SiO_2$ interface.[138] Single-layer $MoS_2$ filed-effect transistors have been utilized to fabricate an integrated small-signal analog amplifier by connecting two top-gated $MoS_2$ transistors in series.[139]

A back-gated double-layer $MoS_2$ field-effect transistor has been fabricated by using titanium contacts. The device shows an ohmic contact at room temperature with a small Schottky barrier, an on/off ratio higher than $10^7$:1, and current saturation. The chemisorption of oxygen and water was found to degrade the conductance values up to 100 times.[140] Transistors have been fabricated using exfoliated $MoS_2$ flakes of different thickness (2–70 nm) and Sc, Ti, Ni, and Pt as metal contacts. Metals with lower work functions such as Sc are effective in improving the contacts, and a 10 nm thick $MoS_2$ sheet with an effective mobility of 700 $cm^2 Vs^{-1}$ is achieved at room temperature.[141] A FET has been made from a sandwich-type structure by using few-layer $MoS_2$ as the semiconducting channel between single-layer graphene and a metal thin film. The on/off ratio is found to be $>10^3$:1 with a high current density of up to 5000 $A cm^{-2}$.[142]

FETs based on sulfides and selenides of tungsten have also been reported. Hwang et al.[143] have reported the fabrication of FETs with few-layer $WS_2$ obtained by sonication in isopropyl alcohol. They demonstrated an ambipolar behavior with a high ($10^5$:1) on/off current ratio and good photoresponse to visible light because of the available band gap in this material. A FET has been fabricated on ultrathin mechanically exfoliated $MoSe_2$ flakes. $MoSe_2$ FETs have n-type characteristics with a mobility of 50 $cm^2 Vs^{-1}$ and on/off ratios larger than $10^6$:1. The strong temperature-dependent mobilities suggest that the phonons are dominant in the scattering mechanism.[144] Podzorov et al.[145] have fabricated FETs of bulk $WSe_2$ with ambipolar characteristics, hole mobilities of 500 $cm^2 Vs^{-1}$, and a high current on/off ratio of $10^5$:1. A FET in the top-gate geometry fabricated on single-layer $WSe_2$ obtained by mechanical exfoliation has a hole mobility of about 250 $cm^2 Vs^{-1}$, an SS value of 60 mV $dec^{-1}$, and an on/off ratio of $10^6$:1 at room temperature.[146]

Room-temperature bottom-gate geometry transistors have been fabricated with GaS and GaSe. The devises based on single sheets of GaS and GaSe show typical n-type and p-type conductance, respectively. Single sheets of GaS and GaSe exhibit field-effect mobilities of 0.1 $cm^2 Vs^{-1}$ and 0.6 $cm^2 Vs^{-1}$, respectively, along with good on/off ratios in the range $10^4$:1–$10^5$:1 (Figure 18).[29a]

## 8. Borocarbonitrides ($B_xC_yN_z$)

Borocarbonitrides are solid materials that are expected to exhibit properties somewhere between insulating BN and conducting graphene, depending on the composition. In the last few years borocarbonitrides have been prepared by different methods, in particular by precursor decomposition or the high-temperature reaction of high-surface-area carbon with boric acid and urea.[147] Most of these materials do not have long-range order in the basal plane or perpendicular to the plane, but generally contain graphene-like segments. Borocarbonitrides can have reasonably extended networks containing BCN rings or domains of BN and graphene.[147] The X-ray photoelectron and electron energy loss spectra as well as the NMR spectra of samples prepared by the urea route show the presence of B–C, B–N, C–C, and C–N bonds.

Extensive first principles calculations have thrown light on the structure and properties of these materials. The

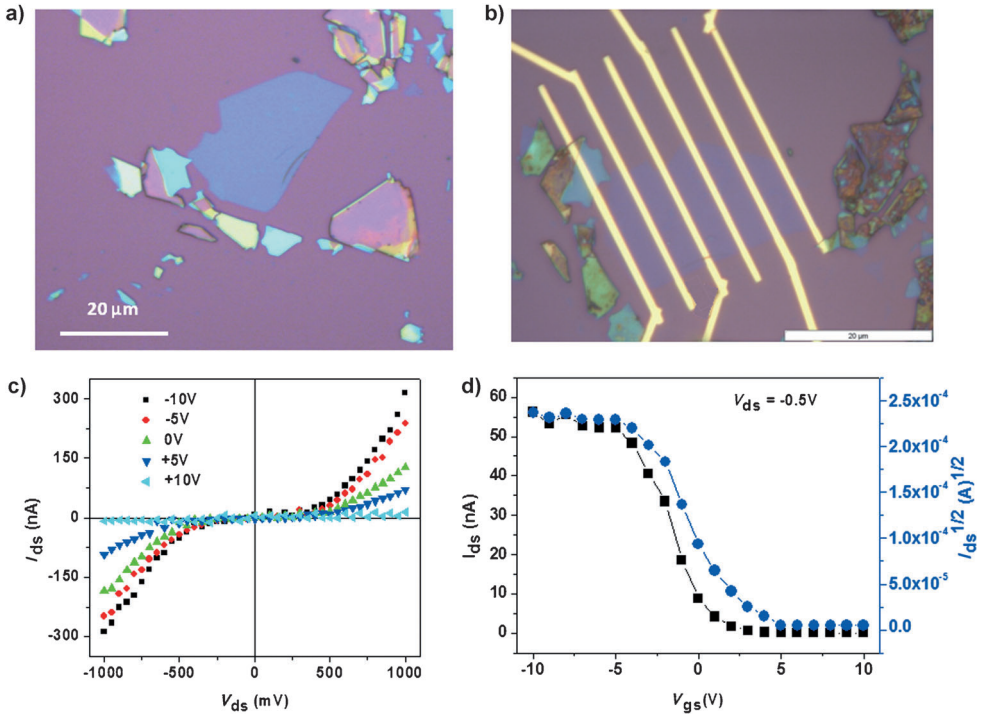


***Figure 18.*** Single-sheet GaSe: a) Typical optical image before patterning the electode and b) optical image after patterning the electrode. c) Room-temperature FET output characteristics of single-sheet GaSe in the dark at constant humidity (22%). d) Transfer characteristics of a GaSe single-sheet FET. (Adapted from Ref. [29a].)

borocarbonitrides prepared by the urea method exhibit large surface areas similar to graphene and also show high $CO_2$ uptake (up to 125 wt% at 195 K). The electrical conductivity of these materials depends on the carbon content, and the compositions with a high carbon content are found to have good characteristics for supercapacitor applications and also appear to exhibit insulator–metal transitions. Figure 19 shows the supercapacitor characteristics of $BC_3N$ and $BC_{4.5}N$, with specific capacitance values of 178 $F g^{-1}$ and 240 $F g^{-1}$ (at a scan rate of 5 $mV s^{-1}$) evident in aqueous and ionic liquid media, respectively.[148] $BC_3N$ and $BC_{4.5}N$ also appear to be good electrode materials for lithium batteries.

## 9. Composites of $MoS_2$ with Graphene and Polymers

Thin-film composites of graphene nanosheets in a matrix of $MoS_2$ nanosheets have been prepared and characterized. Microscopy and spectroscopic studies revealed that the composites were uniform on a micrometer length scale. An increase in conductivity of up to nine orders of magnitude was found on addition of graphene.[149] Nanocomposites of few-layer metal chalcogenides with reduced graphene oxide (RGO) have been prepared by heating the individual components in the presence of hydrazine hydrate at reflux. The XRD patterns and Raman spectra show the features of both $MoS_2$ and RGO. There is a progressive decrease in the resistivity as the proportion of RGO in the composite increases.[23]

In few-layer $MoS_2$-PANI composites, prepared by in situ polymerization of aniline (PANI) with ammonium persulfate in dilute HCl, the polaronic structure of PANI gets stabilized.[23] Hierarchical $MoS_2$/PANI nanowires show improved Li-ion storage properties, with a high charge capacity of 1063.9 $mA h^{-1} g^{-1}$ at a current density of 100 $mA g^{-1}$ and with 90.2% efficiency after 50 cycles.[150] Few-layer $MoS_2$–PVP composites, prepared by sonication of

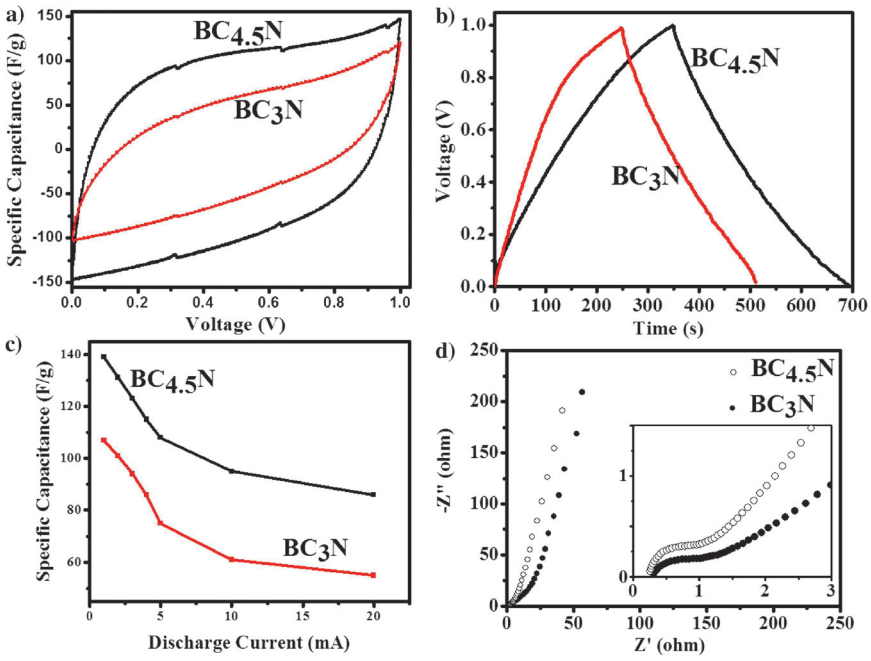


***Figure 19.*** a) Cyclic voltammograms of $BC_{4.5}N$ and $BC_3N$ at a scan rate of 100 $mV s^{-1}$. b) Galvanostatic charge/discharge curves for $BC_{4.5}N$ and $BC_3N$ electrodes at a current density of 100 $mA g^{-1}$. c) Specific capacitance as a function of discharge current. d) Nyquist curves for $BC_{4.5}N$ and $BC_3N$ electrodes. The inset in (d) shows magnified data near the origin. (Adapted from Ref. [148].)

$MoS_2$ and polyvinylpyrolidone (PVP) in ethanol for 9 h, have been used to prepare a device with the configuration RGO/$MoS_2$-PVP/Al for flexible nonvolatile rewritable memory.[151] $MoS_2$/poly(vinyl alcohol) nanocomposites obtained by solvent blending have been examined for their fire resistance and mechanical properties. The improvement in the properties of the nanocomposites is attributed to strong interactions between the PVA and $MoS_2$.[152]

## 10. Applications

### 10.1. Lithium-Ion Batteries

Layered transition-metal dichalcogenides $MX_2$ (M = Mo, Ti, V, and W, X = S, Se) can intercalate and deintercalate Li ions between the layers and also exhibit fast ion conductivity. These features render them good host materials for primary or rechargeable batteries. The first lithium-ion battery using $MoS_2$ as the electrode material was prepared by Haering et al.[153] $MoS_2$ with an enlarged *c*-lattice parameter and surface area obtained by exfoliation shows a first charge capacity of 800 $mA\,h^{-1}\,g^{-1}$, and maintains a capacity of 750 $mA\,h^{-1}\,g^{-1}$ after 20 cycles at a current density of 50 $mA\,g^{-1}$.[154] Bulk $MoS_2$ electrodes show a decrease in their charge capacity from 800 to 226 $mh\,g^{-1}$ after 50 cycles. Feng et al.[155] have found that $MoS_2$ nanoflake electrodes prepared hydrothermally exhibit a capacity of about 1000 $mA\,h^{-1}\,g^{-1}$. Hierarchical spheres composed of ultrathin $MoS_2$ nanosheets prepared by the polystyrene microsphere assisted hydrothermal method show a lithium storage capacity of 672 $mA\,h^{-1}\,g^{-1}$.[156] $MoS_2$ nanoflowers obtained by the ionic-liquid-assisted hydrothermal method show a reversible capacity of about 900 $mA\,h^{-1}\,g^{-1}$.[157] Graphene-like $MoS_2$ nanoplates obtained solvothermaly by using molybdenumcarbonyl and sulfur showed first discharge and charge capacities of 1062 and 917 $mA\,h^{-1}\,g^{-1}$, respectively, at a current density of 1.06 $A\,g^{-1}$.[158]

Julien et al.[159] studied $WS_2$ for electrochemical applications and demonstrated that 0.6 mol Li ions intercalate per mol of $WS_2$. $WS_2$ nanotubes show a reversible capacity of above 500 $mA\,h^{-1}\,g^{-1}$,[160] while co-doped $WS_2$ nanorods reversibly store lithium with a capacity of 568 $mA\,h^{-1}\,g^{-1}$ at a current density of 50 $mA\,g^{-1}$.[161] Feng et al.[162] found that $WS_2$ nanoflakes exhibit a higher reversible charging capacity of 780 $mA\,h^{-1}\,g^{-1}$ with good cycling stability at a current density of 47.5 $mA\,g^{-1}$. Seo et al.[163] reported that $WS_2$ nanosheets obtained by sulfurization of $W_{18}O_{49}$ nanorods exhibit a first reversible discharge capacity of 377 $mA\,h^{-1}\,g^{-1}$ at a current density of 100 $mA\,g^{-1}$. Mesoporous $WS_2$ with a high surface area, synthesized using SBA-15 as the template, has a storage capacity of 805 $mA\,h^{-1}\,g^{-1}$ at a current density of 0.1 $A\,g^{-1}$.[164] The electrochemical performance of the superacid-treated $WS_2$ has a higher reversible first-cycle capacity of 470 $mA\,h^{-1}\,g^{-1}$ at a current density of 25 $mA\,g^{-1}$.[165]

The commercially available anode material for lithium-ion batteries is graphite, which has a relatively small capacity (372 $mA\,h^{-1}\,g^{-1}$).[166] Graphene has been studied extensively for electrochemical applications because of its large surface area and chemical stabilty.[167] It is used as a matrix to improve the electrochemical performance of various nanomaterials, including metal and metal oxides.[32a,168] Extensive research has been carried out on the composites of graphene with inorganic graphene analogues. In situ reduction of $MoO_4^-$ on graphene with thiourea under hydrothermal conditions gave nanoflakes of $MoS_2$ on graphene with a very high capacity for lithiation and delithiation.[169] A highest specific value of the lithiation capacity of 2200 $mA\,h^{-1}\,g^{-1}$ was observed in the first cycle, and with a sustained specific reversible capacity of 1290 $mA\,h^{-1}\,g^{-1}$ at a current density of 100 $mA\,g^{-1}$ up to 50 cycles (Figure 20a). The specific capacity of 1040 $mA\,h^{-1}\,g^{-1}$ was even retained at a high current density of 1000 $mA\,g^{-1}$ (Figure 20b). Das et al.[170] reported that the composites of $MoS_2$ with amorphous carbon obtained by a hydrothermal method have a storage capacity of 800 $mA\,h^{-1}\,g^{-1}$ at a current of 400 $mA\,g^{-1}$. Composites of single-layer $MoS_2$ with graphene and amorphous carbon obtained from a solution-phase method have been used as anode materials with a reversible capacity of 900–1100 $mA\,h^{-1}\,g^{-1}$ with a high cyclic stability at 100 $mA\,g^{-1}$.[34] Graphene-like $MoS_2$/amorphous-carbon composites obtained hydrothermally have a reversible capacity of 912 $mA\,h^{-1}\,g^{-1}$ after 100 cycles.[171] $MoS_2$/graphene composites prepared by the L-cysteine-based solution method, followed by annealing in a $H_2/N_2$ atmosphere at 800 °C for 2 h, show

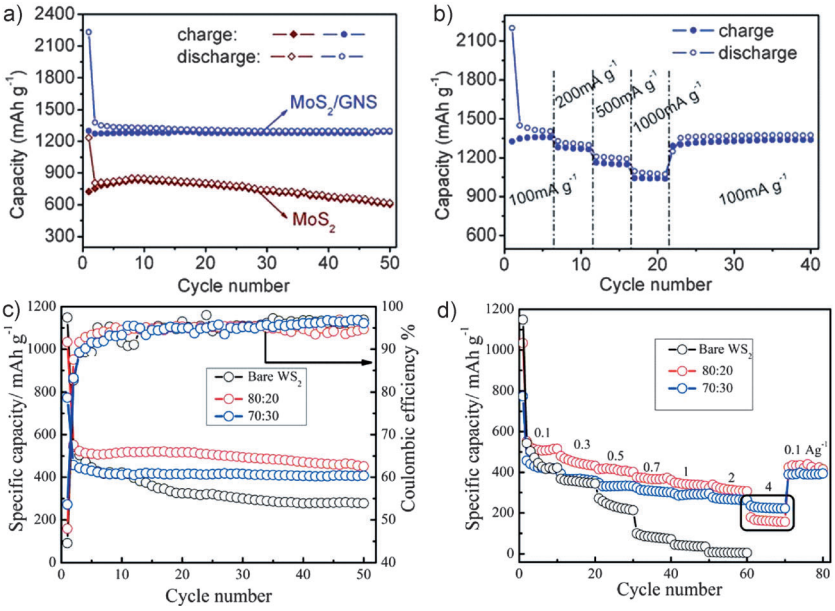


***Figure 20.*** a) Galvanostatic cycling behaviors of $MoS_2$ and $MoS_2$-graphene at a current density of 100 $mA\,g^{-1}$. b) Cycling behavior of $MoS_2$-graphene at different current densities. c) Galvanostatic cycling performance and Coulombic efficiencies of bare $WS_2$ and $WS_2$-graphene composites at a different current density of 100 $mA\,g^{-1}$ and d) the specific capacities at various discharge currents of 0.1, 0.3, 0.5, 0.7, 1, 2, and 4 A g. (Adapted from Refs. [169] and [173].)

a specific capacity of 1100 mA h$^{-1}$ g$^{-1}$ at a current density of 100 mA g$^{-1}$, with no capacity fading even after 100 cycles.[172]

Graphene–$WS_2$ composites prepared by heating the dispersed GO and few-layer $WS_2$ at reflux in water using sodium borohydride as the reducing agent show a high specific capacity and more importantly good stability compared to the pristine $WS_2$. Figure 20c shows the discharge specific capacities and Columbic efficiencies of $WS_2$ and $WS_2$-RGO at a current density of 100 mA g$^{-1}$ for the first 50 cycles. After 50 cycles, the discharge capacity of bare $WS_2$ electrode decreases to 278 mA h$^{-1}$ g$^{-1}$, while that of the composite electrodes is 451 mA h$^{-1}$ g$^{-1}$. The composite retains a high specific capacity at high current densities of up to 4 Ah g$^{-1}$ (Figure 20d). Reduced graphene oxide plays an important role in enhancing the charging rate of $WS_2$-RGO composites.[173]

### 10.2. Catalysts

Layered metal chalcogenides are known to be excellent catalysts for the hydrodesulfurization (HDS) of sulfur-containing aromatic hydrocarbons.[174] $MoS_2$ nanotubes covered with Ni nanoparticles act as catalysts for the hydrodesulfurization of thiophene and its derivatives at relatively low temperatures, with conversion efficiencies up to 96%.[175] Tenne et al.[176] reported that $WS_2$ nanotubes covered with cobalt nanoparticles exhibit a catalytic conversion of about 12% for the HDS of thiophene at 600°C. The hydrodesulfurization of thiophene has been carried out on single-layer $MoS_2$ clusters, with metallic brim sites being considered important for the reaction.[174b] Recently, a detailed study has been carried out on few-layer $MoS_2$ as a catalyst for the HDS of thiophene. The effect of Co and Ni nanoparticles decorating few-layer $MoS_2$ was also studied. Few-layer $MoS_2$ shows superior performance compared to bulk $MoS_2$ and $MoS_2$ nanotubes, with the conversion being 64% at 450°C (Figure 21). $MoS_2$ sheets decorated with Co or Ni nanoparticles show a conversion of 98% at 375°C.[177] A composite of Ni-Fe/$MoS_2$ with a molar ratio of 80:20 shows good electrocatalytic activity toward the oxidation of hydrazine.[178]

Hinemenn et al.[179] proposed that $MoS_2$ nanoparticles would be good catalysts with a moderate overpotential of 0.1 V–0.2 V for hydrogen evolution reactions (HER). Jaramillo et al.[180] synthesized pentagonal-shaped, atomically thin $MoS_2$ on Au(111) and studied the electrochemical exchange current density as a function of the $MoS_2$ edge length. The edge sites of $MoS_2$ were found to be active for the HER. First-principles density functional theory and finite-temperature molecular dynamics calculations show that vacancy defects in single-layer $MoS_2$ are active for $H_2O$ dissociation and $H_2$ production.[181] On the basis of such predictions, there has been an upsurge in research activity of the HER reaction by using $MoS_2$ in both electrochemical and photocatalytic reactions.[182] Amorphous $MoS_2$ films prepared on FTO-coated glass by electropolymerization (FTO = fluorine-doped tin oxide) are more active than single-crystalline and nanoparticulate $MoS_2$ for the HER. The Tafel slope of amorphous $MoS_2$ film was 40 mV per decade, while for nanoparticles and

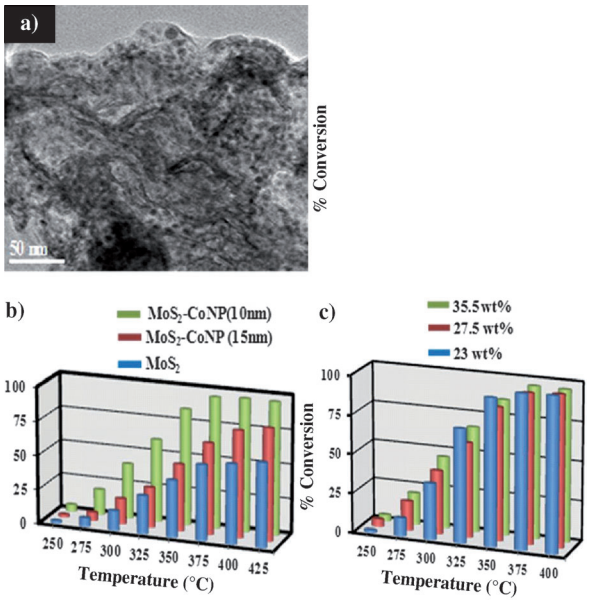


***Figure 21.*** a) Few-layer $MoS_2$ decorated with 10 nm cobalt nanoparticles. b) Temperature dependence of the conversion of thiophene over few-layer $MoS_2$ decorated with 10 and 15 nm cobalt nanoparticles. c) Temperature dependence of the conversion of thiophene at different loadings of 10 nm cobalt nanoparticles. (Adapted from Ref. [177].)

single crystals the values were 60 mV and 120 mV per decade, respectively.[183] Nanosheets of $WS_2$ prepared by ball milling $WO_3$ and S followed by annealing at 600°C shows a higher HER activity compared to bulk $WS_2$.[184] The necessary criterion for good electrocatalytic activity with such sulfides is the greater degree of exposure of the catalytically active edge sites. Kibsgaard et al.[185] have developed large-area continuous thin films of highly ordered mesoporous $MoS_2$ and showed that the HER activity is better than that of flat $MoS_2$ and $MoS_2$ nanowires. Lau et al.[186] used ionic liquids to synthesize porous $MoS_2$ nanosheets with a large proportion of edges and found an increased HER catalytic activity. Hydrothermally synthesized graphene–$MoS_2$ composites containing nanoscopic few-layer $MoS_2$ show much higher HER activity (Tafel slope 41 mV per decade) at a low onset potential of 0.15 V versus RHE compared to $MoS_2$.[187] Edge sites along with good electrical coupling to graphene are responsible for the high activity.[188]

As a consequence of their small indirect band gaps, $MoS_2$ and $WS_2$ do not act as photocatalysts for $H_2$ evolution. Photocatalytic evolution of $H_2$ can be enhanced by attaching a good photon absorber such as CdS, CdSe, $TiO_2$, and even molecular systems such as [Ru(bpy)$_3$] (bpy = bipyridine) and eyosin. $TiO_2$ nanobelts coated with $MoS_2$ nanoflakes result in a high photocatalytic hydrogen production of 1.6 mmol hgm$^{-1}$ with 50 wt% $MoS_2$ loading.[189] The incorporation of graphene in the composite results in the catalytic activity increasing to a quantum efficiency of 9.7% at 365 nm. Graphene acts as an electron collector and enhances charge separation, while $MoS_2$ provides active sites for the HER.[190] Photocatalytic $H_2$ evolution has been achieved using $MoS_2$ grown on CdS. The catalytic activity of CdS increases by 36 times with a loading of just 0.2 wt% $MoS_2$ nanosheets.[191] $MoS_2$ nanosheets grown

on CdSe ribbons show good photocatalytic activity under visible light.[192] Tran et al.[193] prepared photocathodes by the electrodeposition of $MoS_2$ on Si nanowires and found hydrogen evolution with an onset anodic potential shift of 200 mV under irradiation with visible light in an aqueous solution at pH 5.0. Hydrogen evolution can be achieved in $MoS_2$ by dye sensitization. Graphene–$MoS_2$ composites sensitized with eosin Y show hydrogen evolution with an apparent quantum efficiency (AQE) of 24% at 460 nm.[194]

### 10.3. Sensors and Radiation Detectors

Mechanically exfoliated $MoS_2$ nanosheets with one to four layers in a transistor geometry have been used to detect 2 ppm NO, whereby there is an 80% decrease in the channel conductance.[195] A flexible thin-film transistor has been devised for sensing $NO_2$ gas by using a $MoS_2$ thin film as the channel and RGO as the electrode material. A thin film of $MoS_2$ covered with Pt nanoparticles increases the sensitivity approximately three times with a detection limit of 2 ppb.[196] Electrochemically reduced $MoS_2$ shows good conductivity and fast electron transfer and can be used for the selective detection of dopamine and glucose.[197] Transistors based on one to six layers of $MoS_2$ are found to be good sensors for $NH_3$, $H_2S$, and humidity.[198]

Single-, double-, and triple-layer $MoS_2$ obtained by mechanical exfoliation has been used for phototransistors in the top-gate geometry. The phototransistors with single- and double-layer $MoS_2$ have been used for the detection of green light, whereas the triple-layer $MoS_2$ is found to be effective for the detection of red light.[199] Recently, $MoS_2$ with a thickness in the range 10–60 nm has been used for the successful detection of UV to near-IR radiation.[200] Nanosheets of $MoS_2$ and $MoSe_2$ are good IR radiation detectors, comparable to reduced graphene oxide.[1e]

### 10.4. Mechanical Properties

Single- and double-layer $MoS_2$ mechanically exfoliated from bulk $MoS_2$ and transferred to a substrate with an array of microfabricated circular holes have been studied by atomic force microscopy. The in-plane stiffness of single-layer $MoS_2$ was $(180 \pm 60)\ N\,m^{-1}$, which corresponds to an effective Young's modulus of $(270 \pm 100)$ GPa, which is comparable to that of steel. The breaking strength or Young's modulus (%) of 11%, corresponds to the upper theoretical limit and indicates that the material is highly crystalline and defect-free.[201] Castellanos-Gomez et al.[202] obtained an average effective Young's modulus of $(330 \pm 70)$ GPa for $MoS_2$ nanosheets having 5 to 25 layers. Theoretical studies have provided insight into the failure of this mechanism. The tensile strength of single-layer $MoS_2$ is governed by the instability of the out-of-plane soft-mode phonon under biaxial tension and uniaxial tension in the armchair direction.[203] $MoS_2$ nanosheets with lateral dimensions of 0.7 μm and 2–5 μm obtained by varying the sonication times and centrifugion degrade the mechanical properties of PVA with an E value of 1.6 GPa, whereas the larger flakes improved the performance, having a Young modulus of 3.2 GPa compared with the Young's modulus of 2.8 GPa for PVA.[11] BN nanosheets with different numbers of layers have been incorporated into polymers to prepare composites. The elastic modulus and hardness both increase as the sheet thickness decreases.[204] Figure 22 shows the variation in hardness and elastic modulus of BN films as a function of urea and boric acid ratio, which directly determines the number of layers. It must be noted that fracture toughness is the more relevant property of nanocomposites.

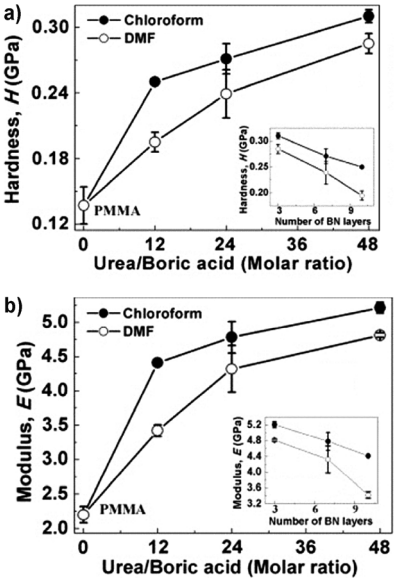


*Figure 22.* Variation of the a) hardness and b) elastic modulus of BN-PMMA composites prepared in chloroform and DMF as solvents as a function of the boric acid to urea ratio used for the synthesis of BN. PMMA = polymethylmethacrylate. The insets show the variations in hardness and elastic modulus as a function of number of BN layers. (Adapted from Ref. [204].)

## 11. Outlook

The previous sections covering the synthesis, characterization, properties, and applications of a variety of graphene-like layered inorganic materials should indicate the novelty of these materials. Just as graphene is finding several applications in a variety of areas, it appears likely that single- and few-layered materials formed by some of the inorganic compounds will similarly find many uses. It is noteworthy that field-effect transistors, sensors, radiation detectors, and supercapacitors based on these materials have already been reported. It is also likely that single- and few-layered structures of a variety of inorganic materials other than those discussed in this Review will be prepared in the future, with many of them exhibiting properties of great interest. Composites formed by the inorganic sheets themselves or with polymers, graphene, and other materials need to be explored. It should be possible to prepare interesting

structures such as metal–organic frameworks by incorporating nanosheets of BN and other materials.

Received: February 22, 2013
Published online: October 11, 2013

[1] a) K. S. Novoselov, A. K. Geim, S. V. Morozov, D. Jiang, Y. Zhang, S. V. Dubonos, I. V. Grigorieva, A. A. Firsov, *Science* **2004**, *306*, 666 – 669; b) K. S. Novoselov, A. K. Geim, S. V. Morozov, D. Jiang, M. I. Katsnelson, I. V. Grigorieva, S. V. Dubonos, A. A. Firsov, *Nature* **2005**, *438*, 197 – 200; c) A. K. Geim, K. S. Novoselov, *Nat. Mater.* **2007**, *6*, 183 – 191; d) C. N. R. Rao, A. K. Sood, K. S. Subrahmanyam, A. Govindaraj, *Angew. Chem.* **2009**, *121*, 7890 – 7916; *Angew. Chem. Int. Ed.* **2009**, *48*, 7752 – 7777; e) C. N. R. Rao, H. S. S. R. Matte, K. S. Subrahmanyam, *Acc. Chem. Res.* **2013**, *46*, 149 – 159.

[2] a) K. S. Novoselov, D. Jiang, F. Schedin, T. J. Booth, V. V. Khotkevich, S. V. Morozov, A. K. Geim, *Proc. Natl. Acad. Sci. USA* **2005**, *102*, 10451 – 10453; b) C. N. R. Rao, A. Nag, *Eur. J. Inorg. Chem.* **2010**, 4244 – 4250; c) K. Raidongia, A. Gomathi, C. N. R. Rao, *Israel J. Chem.* **2010**, *50*, 399 – 404; d) R. Mas-Ballesté, C. Gómez-Navarro, J. Gómez-Herrero, F. Zamora, *Nanoscale* **2011**, *3*, 20 – 30; e) X. Huang, Z. Zeng, H. Zhang, *Chem. Soc. Rev.* **2013**, *42*, 1934 – 1946; f) M. Xu, T. Liang, M. Shi, H. Chen, *Chem. Rev.* **2013**, *113*, 3766 – 3798; g) Q. H. Wang, K. Kalantar-Zadeh, A. Kis, J. N. Coleman, M. S. Strano, *Nat. Nanotechnol.* **2012**, *7*, 699 – 712; h) M. Chhowalla, H. S. Shin, G. Eda, L.-J. Li, K. P. Loh, H. Zhang, *Nat. chem.* **2013**, *5*, 263 – 275; i) X. Song, J. Hu, H. Zeng, *J. Mater. Chem. C* **2013**, *1*, 2952 – 2969.

[3] C. N. R. Rao, A. K. Sood, R. Voggu, K. S. Subrahmanyam, *J. Phys. Chem. Lett.* **2010**, *1*, 572 – 580.

[4] J. N. Coleman, M. Lotya, A. O'Neill, S. D. Bergin, P. J. King, U. Khan, K. Young, A. Gaucher, S. De, R. J. Smith, I. V. Shvets, S. K. Arora, G. Stanton, H.-Y. Kim, K. Lee, G. T. Kim, G. S. Duesberg, T. Hallam, J. J. Boland, J. J. Wang, J. F. Donegan, J. C. Grunlan, G. Moriarty, A. Shmeliov, R. J. Nicholls, J. M. Perkins, E. M. Grieveson, K. Theuwissen, D. W. McComb, P. D. Nellist, V. Nicolosi, *Science* **2011**, *331*, 568 – 571.

[5] R. G. Dickinson, L. Pauling, *J. Am. Chem. Soc.* **1923**, *45*, 1466 – 1471.

[6] R. F. Frindt, *J. Appl. Phys.* **1966**, *37*, 1928 – 1929.

[7] P. Joensen, R. F. Frindt, S. R. Morrison, *Mater. Res. Bull.* **1986**, *21*, 457 – 461.

[8] B. K. Miremadi, S. R. Morrison, *J. Appl. Phys.* **1988**, *63*, 4970 – 4974.

[9] a) D. Yang, R. F. Frindt, *J. Phys. Chem. Solids* **1996**, *57*, 1113 – 1116; b) A. Koma, K. Yoshimura, *Surf. Sci.* **1986**, *174*, 556 – 560.

[10] D. Yang, S. J. Sandoval, W. M. R. Divigalpitiya, J. C. Irwin, R. F. Frindt, *Phys. Rev. B* **1991**, *43*, 12053 – 12056.

[11] A. O'Neill, U. Khan, J. N. Coleman, *Chem. Mater.* **2012**, *24*, 2414 – 2421.

[12] K.-G. Zhou, N.-N. Mao, H.-X. Wang, Y. Peng, H.-L. Zhang, *Angew. Chem.* **2011**, *123*, 11031 – 11034; *Angew. Chem. Int. Ed.* **2011**, *50*, 10839 – 10842.

[13] Y. Yao, Z. Lin, Z. Li, X. Song, K.-S. Moon, C.-p. Wong, *J. Mater. Chem.* **2012**, *22*, 13494 – 13499.

[14] a) H. S. S. R. Matte, A. Gomathi, A. K. Manna, D. J. Late, R. Datta, S. K. Pati, C. N. R. Rao, *Angew. Chem.* **2010**, *122*, 4153 – 4156; *Angew. Chem. Int. Ed.* **2010**, *49*, 4059 – 4062; b) H. S. S. R. Matte, B. Plowman, R. Datta, C. N. R. Rao, *Dalton Trans.* **2011**, *40*, 10322 – 10325.

[15] Z. Zeng, Z. Yin, X. Huang, H. Li, Q. He, G. Lu, F. Boey, H. Zhang, *Angew. Chem.* **2011**, *123*, 11289 – 11293; *Angew. Chem. Int. Ed.* **2011**, *50*, 11093 – 11097.

[16] Z. Zeng, T. Sun, J. Zhu, X. Huang, Z. Yin, G. Lu, Z. Fan, Q. Yan, H. H. Hng, H. Zhang, *Angew. Chem.* **2012**, *124*, 9186 – 9190; *Angew. Chem. Int. Ed.* **2012**, *51*, 9052 – 9056.

[17] K.-K. Liu, W. Zhang, Y.-H. Lee, Y.-C. Lin, M.-T. Chang, C.-Y. Su, C.-S. Chang, H. Li, Y. Shi, H. Zhang, C.-S. Lai, L.-J. Li, *Nano Lett.* **2012**, *12*, 1538 – 1544.

[18] Y.-H. Lee, X.-Q. Zhang, W. Zhang, M.-T. Chang, C.-T. Lin, K.-D. Chang, Y.-C. Yu, J. T.-W. Wang, C.-S. Chang, L.-J. Li, T.-W. Lin, *Adv. Mater.* **2012**, *24*, 2320 – 2325.

[19] V. O. Koroteev, L. G. Bulusheva, A. V. Okotrub, N. F. Yudanov, D. V. Vyalikh, *Phys. Status Solidi B* **2011**, *248*, 2740 – 2743.

[20] Y. Zhan, Z. Liu, S. Najmaei, P. M. Ajayan, J. Lou, *Small* **2012**, *8*, 966 – 971.

[21] D. Kim, D. Sun, W. Lu, Z. Cheng, Y. Zhu, D. Le, T. S. Rahman, L. Bartels, *Langmuir* **2011**, *27*, 11650 – 11653.

[22] Y.-C. Lin, W. Zhang, J.-K. Huang, K.-K. Liu, Y.-H. Lee, C.-T. Liang, C.-W. Chu, L.-J. Li, *Nanoscale* **2012**, *4*, 6637 – 6641.

[23] H. S. S. R. Matte, U. Maitra, P. Kumar, B. G. Rao, K. Pramoda, C. N. R. Rao, *Z. Anorg. Allg. Chem.* **2012**, *638*, 2617 – 2624.

[24] C. Altavilla, M. Sarno, P. Ciambelli, *Chem. Mater.* **2011**, *23*, 3879 – 3885.

[25] A. Castellanos-Gomez, M. Barkelid, A. M. Goossens, V. E. Calado, H. S. J. van der Zant, G. A. Steele, *Nano Lett.* **2012**, *12*, 3187 – 3192.

[26] K. Gacem, M. Boukhicha, Z. Chen, A. Shukla, *Nanotechnology* **2012**, *23*, 505709.

[27] S. Jeong, D. Yoo, J.-T. Jang, M. Kim, J. Cheon, *J. Am. Chem. Soc.* **2012**, *134*, 18233 – 18236.

[28] D. J. Late, B. Liu, H. S. S. R. Matte, C. N. R. Rao, V. P. Dravid, *Adv. Funct. Mater.* **2012**, *22*, 1894 – 1905.

[29] a) D. J. Late, B. Liu, J. Luo, A. Yan, H. S. S. R. Matte, M. Grayson, C. N. R. Rao, V. P. Dravid, *Adv. Mater.* **2012**, *24*, 3549 – 3554; b) P. Hu, Z. Wen, L. Wang, P. Tan, K. Xiao, *ACS Nano* **2012**, *6*, 5988 – 5994.

[30] U. K. Gautam, S. R. C. Vivekchand, A. Govindaraj, C. N. R. Rao, *Chem. Commun.* **2005**, 3995 – 3997.

[31] D.-J. Xue, J. Tan, J.-S. Hu, W. Hu, Y.-G. Guo, L.-J. Wan, *Adv. Mater.* **2012**, *24*, 4528 – 4533.

[32] a) T. Gao, T. Wang, *Cryst. Growth Des.* **2010**, *10*, 4995 – 5000; b) Y. Yu, Y. Bin, G. Zhiwei, M. Hu, Z. Hui, D. Lun, Q. Guogang, *Nanotechnology* **2012**, *23*, 194004.

[33] J. Feng, L. Peng, C. Wu, X. Sun, S. Hu, C. Lin, J. Dai, J. Yang, Y. Xie, *Adv. Mater.* **2012**, *24*, 1969 – 1974.

[34] J. Feng, X. Sun, C. Wu, L. Peng, C. Lin, S. Hu, J. Yang, Y. Xie, *J. Am. Chem. Soc.* **2011**, *133*, 17832 – 17838.

[35] X. Zhang, J. Zhang, J. Zhao, B. Pan, M. Kong, J. Chen, Y. Xie, *J. Am. Chem. Soc.* **2012**, *134*, 11908 – 11911.

[36] H. Li, G. Lu, Y. Wang, Z. Yin, C. Cong, Q. He, L. Wang, F. Ding, T. Yu, H. Zhang, *Small* **2012**, *9*, 1974 – 1981.

[37] C. Li, L. Huang, G. P. Snigdha, Y. Yu, L. Cao, *ACS Nano* **2012**, *6*, 8868 – 8877.

[38] D. D. Vaughn II, R. J. Patel, M. A. Hickner, R. E. Schaak, *J. Am. Chem. Soc.* **2010**, *132*, 15170 – 15172.

[39] Y. Zhang, J. Lu, S. Shen, H. Xu, Q. Wang, *Chem. Commun.* **2011**, *47*, 5226 – 5228.

[40] D. D. Vaughn, S.-I. In, R. E. Schaak, *ACS Nano* **2011**, *5*, 8852 – 8860.

[41] C. Zhai, N. Du, H. Z. D. Yang, *Chem. Commun.* **2011**, *47*, 1270 – 1272.

[42] H. Zhong, G. Yang, H. Song, Q. Liao, H. Cui, P. Shen, C.-X. Wang, *J. Phys. Chem. C* **2012**, *116*, 9319 – 9326.

[43] Z. Fang, Q. Wang, X. Wang, B. Zhu, F. Fan, C. Wang, X. Liu, *Cryst. Res. Technol.* **2012**, *47*, 635 – 642.

[44] S. Acharya, M. Dutta, S. Sarkar, D. Basak, S. Chakraborty, N. Pradhan, *Chem. Mater.* **2012**, *24*, 1779 – 1785.

[45] G.-H. Dong, Y.-J. Zhu, G.-F. Cheng, Y.-J. Ruan, *J. Alloys Compd.* **2013**, *550*, 164 – 168.

[46] Y. Min, G. D. Moon, B. S. Kim, B. Lim, J.-S. Kim, C. Y. Kang, U. Jeong, *J. Am. Chem. Soc.* **2012**, *134*, 2872 – 2875.
[47] D. Teweldebrhan, V. Goyal, A. A. Balandin, *Nano Lett.* **2010**, *10*, 1209 – 1218.
[48] Y. Zhao, R. W. Hughes, Z. Su, W. Zhou, D. H. Gregory, *Angew. Chem.* **2011**, *123*, 10581 – 10585; *Angew. Chem. Int. Ed.* **2011**, *50*, 10397 – 10401.
[49] G. Hao, X. Qi, Y. Liu, Z. Huang, H. Li, K. Huang, J. Li, L. Yang, J. Zhong, *J. Appl. Phys.* **2012**, *111*, 114312 – 114315.
[50] C. Ataca, H. Şahin, S. Ciraci, *J. Phys. Chem. C* **2012**, *116*, 8983 – 8999.
[51] H.-P. Komsa, A. V. Krasheninnikov, *J. Phys. Chem. Lett.* **2012**, *3*, 3652 – 3656.
[52] X.-D. Wen, R. Hoffmann, N. W. Ashcroft, *Adv. Mater.* **2013**, *25*, 261 – 266.
[53] Y. Ma, Y. Dai, M. Guo, C. Niu, J. Lu, B. Huang, *Phys. Chem. Chem. Phys.* **2011**, *13*, 15546 – 15553.
[54] Y. Ma, Y. Dai, M. Guo, C. Niu, Y. Zhu, B. Huang, *ACS Nano* **2012**, *6*, 1695 – 1701.
[55] Y. Lin, J. W. Connell, *Nanoscale* **2012**, *4*, 6908 – 6939.
[56] a) A. Nagashima, N. Tejima, Y. Gamou, T. Kawai, C. Oshima, *Phys. Rev. B* **1995**, *51*, 4606 – 4613; b) A. B. Preobrajenski, A. S. Vinogradov, N. Martensson, *Surf. Sci.* **2005**, *582*, 21 – 30.
[57] M. Corso, W. Auwärter, M. Muntwiler, A. Tamai, T. Greber, J. Osterwalder, *Science* **2004**, *303*, 217 – 220.
[58] a) W. Auwärter, H. U. Suter, H. Sachdev, T. Greber, *Chem. Mater.* **2004**, *16*, 343 – 345; b) F. Müller, K. Stöwe, H. Sachdev, *Chem. Mater.* **2005**, *17*, 3464 – 3467.
[59] D. Pacilé, J. C. Meyer, C. Ö. Girit, A. Zettl, *Appl. Phys. Lett.* **2008**, *92*, 133107 – 133103.
[60] N. Alem, R. Erni, C. Kisielowski, M. D. Rossell, W. Gannett, A. Zettl, *Phys. Rev. B* **2009**, *80*, 155425.
[61] J. C. Meyer, A. Chuvilin, G. Algara-Siller, J. Biskupek, U. Kaiser, *Nano Lett.* **2009**, *9*, 2683 – 2689.
[62] a) Y. Lin, T. V. Williams, J. W. Connell, *J. Phys. Chem. Lett.* **2009**, *1*, 277 – 283; b) J. Y. Huang, H. Yasuda, H. Mori, *J. Am. Ceram. Soc.* **2000**, *83*, 403 – 409; c) L. H. Li, Y. Chen, G. Behan, H. Zhang, M. Petravic, A. M. Glushenkov, *J. Mater. Chem.* **2011**, *21*, 11862 – 11866.
[63] X. Chen, J. F. Dobson, C. L. Raston, *Chem. Commun.* **2012**, *48*, 3703 – 3705.
[64] H. Yurdakul, Y. Göncü, O. Durukan, A. Akay, A. T. Seyhan, N. Ay, S. Turan, *Ceram. Int.* **2012**, *38*, 2187 – 2193.
[65] a) W.-Q. Han, L. Wu, Y. Zhu, K. Watanabe, T. Taniguchi, *Appl. Phys. Lett.* **2008**, *93*, 223103; b) C. Zhi, Y. Bando, C. Tang, H. Kuwahara, D. Golberg, *Adv. Mater.* **2009**, *21*, 2889 – 2893; c) Y. Lin, T. V. Williams, J. W. Connell, *J. Phys. Chem. Lett.* **2009**, *1*, 277 – 283.
[66] Y. Lin, T. V. Williams, T.-B. Xu, W. Cao, H. E. Elsayed-Ali, J. W. Connell, *J. Phys. Chem. C* **2011**, *115*, 2679 – 2685.
[67] Ref. [65a].
[68] Z. Zhao, Z. Yang, Y. Wen, Y. Wang, *J. Am. Ceram. Soc.* **2011**, *94*, 4496 – 4501.
[69] a) D. Fujita, T. Homma, *J. Vac. Sci. Technol. A* **1988**, *6*, 230 – 234; b) K. Yoshihara, M. Tosa, K. Nii, *J. Vac. Sci. Technol. A* **1985**, *3*, 1804 – 1808; c) Y. Minami, A. Tohyama, T. Yamada, *J. Vac. Sci. Technol. A* **1989**, *7*, 1585 – 1588.
[70] M. Xu, D. Fujita, H. Chen, N. Hanagata, *Nanoscale* **2011**, *3*, 2854 – 2858.
[71] a) L. Song, L. Ci, H. Lu, P. B. Sorokin, C. Jin, J. Ni, A. G. Kvashnin, D. G. Kvashnin, J. Lou, B. I. Yakobson, P. M. Ajayan, *Nano Lett.* **2010**, *10*, 3209 – 3215; b) H. Hiura, H. Miyazaki, K. Tsukagoshi, *Appl. Phys. Express* **2010**, *3*, 095101; c) K. H. Lee, H.-J. Shin, J. Lee, I.-Y. Lee, G.-H. Kim, J.-Y. Choi, S.-W. Kim, *Nano Lett.* **2012**, *12*, 714 – 718.
[72] S. Chatterjee, Z. Luo, M. Acerce, D. M. Yates, A. T. C. Johnson, L. G. Sneddon, *Chem. Mater.* **2011**, *23*, 4414 – 4416.
[73] L. Qin, J. Yu, M. Y. Li, F. Liu, X. Bai, *Nanotechnology* **2011**, *22*, 215602.
[74] a) Z. Liu, L. Song, S. Zhao, J. Huang, L. Ma, J. Zhang, J. Lou, P. M. Ajayan, *Nano Lett.* **2011**, *11*, 2032 – 2037; b) K. K. Kim, A. Hsu, X. Jia, S. M. Kim, Y. Shi, M. Hofmann, D. Nezich, J. F. Rodriguez-Nieva, M. Dresselhaus, T. Palacios, J. Kong, *Nano Lett.* **2012**, *12*, 161 – 166.
[75] W.-Q. Han, H.-G. Yu, Z. Liu, *Appl. Phys. Lett.* **2011**, *98*, 203112 – 203113.
[76] A. Pakdel, C. Zhi, Y. Bando, T. Nakayama, D. Golberg, *ACS Nano* **2011**, *5*, 6507 – 6515.
[77] A. Nag, K. Raidongia, K. P. S. S. Hembram, R. Datta, U. V. Waghmare, C. N. R. Rao, *ACS Nano* **2010**, *4*, 1539 – 1544.
[78] X. Wang, C. Zhi, L. Li, H. Zeng, C. Li, M. Mitome, D. Golberg, Y. Bando, *Adv. Mater.* **2011**, *23*, 4072 – 4076.
[79] P. Sutter, J. Lahiri, P. Zahl, B. Wang, E. Sutter, *Nano Lett.* **2013**, *13*, 276 – 281.
[80] M. Osada, T. Sasaki, *Adv. Mater.* **2012**, *24*, 210 – 228.
[81] T. Sasaki, M. Watanabe, *J. Am. Chem. Soc.* **1998**, *120*, 4682 – 4689.
[82] a) R. A. M. Ram, P. Ganguly, C. N. R. Rao, *J. Solid State Chem.* **1987**, *70*, 82 – 87; b) C. N. R. Rao, P. Ganguly, K. K. Singh, R. A. M. Ram, *J. Solid State Chem.* **1988**, *72*, 14 – 23.
[83] Z. Fan, J. Yan, L. Zhi, Q. Zhang, T. Wei, J. Feng, M. Zhang, W. Qian, F. Wei, *Adv. Mater.* **2010**, *22*, 3723 – 3728.
[84] J. S. Chen, X. W. Lou, *Mater. Today* **2012**, *15*, 246 – 254.
[85] G. Pacchioni, *Chem. Eur. J.* **2012**, *18*, 10144 – 10158.
[86] R. Ma, T. Sasaki, *Adv. Mater.* **2010**, *22*, 5082 – 5104.
[87] M. B. Sreedhara, H. S. S. R. Matte, C. N. R. Rao, *Chem. Asian J.* **2013**, *8*, 2430 – 2435.
[88] a) A. K. Cheetham, G. Férey, T. Loiseau, *Angew. Chem.* **1999**, *111*, 3466 – 3492; *Angew. Chem. Int. Ed.* **1999**, *38*, 3268 – 3292; b) C. N. R. Rao, S. Natarajan, R. Vaidhyanathan, *Angew. Chem.* **2004**, *116*, 1490 – 1521; *Angew. Chem. Int. Ed.* **2004**, *43*, 1466 – 1496; c) G. Férey, *Chem. Soc. Rev.* **2008**, *37*, 191 – 214; d) R. Murugavel, A. Choudhury, M. G. Walawalkar, R. Pothiraja, C. N. R. Rao, *Chem. Rev.* **2008**, *108*, 3549 – 3655; e) C. N. R. Rao, J. N. Behera, M. Dan, *Chem. Soc. Rev.* **2006**, *35*, 375 – 387.
[89] a) P.-Z. Li, Y. Maeda, Q. Xu, *Chem. Commun.* **2011**, *47*, 8436 – 8438; b) J.-C. Tan, P. J. Saines, E. G. Bithell, A. K. Cheetham, *ACS Nano* **2012**, *6*, 615 – 621.
[90] M. Moirangthem, P. E. Prasan, C. N. R. Rao, Unpublished results.
[91] a) A. C. Ferrari, J. C. Meyer, V. Scardaci, C. Casiraghi, M. Lazzeri, F. Mauri, S. Piscanec, D. Jiang, K. S. Novoselov, S. Roth, A. K. Geim, *Phys. Rev. Lett.* **2006**, *97*, 187401; b) S. K. Pati, T. Enoki, C. N. R. Rao, *Graphene and its facinating attributes*, World Scientific, Singapore, **2011**.
[92] a) T. J. Wieting, J. L. Verble, *Phys. Rev. B* **1971**, *3*, 4286 – 4292; b) J. M. Chen, C. S. Wang, *Solid State Commun.* **1974**, *14*, 857 – 860; c) P. A. Bertrand, *Phys. Rev. B* **1991**, *44*, 5745 – 5749.
[93] C. Lee, H. Yan, L. E. Brus, T. F. Heinz, J. Hone, S. Ryu, *ACS Nano* **2010**, *4*, 2695 – 2700.
[94] G. Plechinger, S. Heydrich, J. Eroms, D. Weiss, C. Schuller, T. Korn, *Appl. Phys. Lett.* **2012**, *101*, 101906.
[95] H. Li, Q. Zhang, C. C. R. Yap, B. K. Tay, T. H. T. Edwin, A. Olivier, D. Baillargeat, *Adv. Funct. Mater.* **2012**, *22*, 1385 – 1390.
[96] S. Najmaei, Z. Liu, P. M. Ajayan, J. Lou, *Appl. Phys. Lett.* **2012**, *100*, 013106.
[97] C. Ataca, M. Topsakal, E. Aktürk, S. Ciraci, *J. Phys. Chem. C* **2011**, *115*, 16354 – 16361.
[98] A. Molina-Sánchez, L. Wirtz, *Phys. Rev. B* **2011**, *84*, 155413.
[99] a) T. Sekine, K. Uchinokura, T. Nakashizu, E. Matsuura, R. Yoshizaki, *J. Phys. Soc. Jpn.* **1984**, *53*, 811 – 818; b) T. Livneh, E. Sterer, *Phys. Rev. B* **2010**, *81*, 195209.
[100] J. L. Verble, T. J. Wieting, *Phys. Rev. Lett.* **1970**, *25*, 362 – 365.

  

[101] B. Chakraborty, H. S. S. R. Matte, A. K. Sood, C. N. R. Rao, *J. Raman Spectrosc.* **2012**, DOI: 10.1002/jrs.4147.
[102] J. A. Wilson, A. D. Yoffe, *Adv. Phys.* **1969**, *18*, 193 – 335.
[103] a) A. Splendiani, L. Sun, Y. Zhang, T. Li, J. Kim, C.-Y. Chim, G. Galli, F. Wang, *Nano Lett.* **2010**, *10*, 1271 – 1275; b) K. F. Mak, C. Lee, J. Hone, J. Shan, T. F. Heinz, *Phys. Rev. Lett.* **2010**, *105*, 136805; c) T. Korn, S. Heydrich, M. Hirmer, J. Schmutzler, C. Schuller, *Appl. Phys. Lett.* **2011**, *99*, 102109.
[104] a) R. Coehoorn, C. Haas, R. A. de Groot, *Phys. Rev. B* **1987**, *35*, 6203 – 6206; b) R. Coehoorn, C. Haas, J. Dijkstra, C. J. F. Flipse, R. A. de Groot, A. Wold, *Phys. Rev. B* **1987**, *35*, 6195 – 6202.
[105] G. Eda, H. Yamaguchi, D. Voiry, T. Fujita, M. Chen, M. Chhowalla, *Nano Lett.* **2011**, *11*, 5111 – 5116.
[106] W. Zhao, Z. Ghorannevis, L. Chu, M. Toh, C. Kloc, P.-H. Tan, G. Eda, *ACS Nano* **2013**, *7*, 791 – 797.
[107] A. Ramasubramaniam, D. Naveh, E. Towe, *Phys. Rev. B* **2011**, *84*, 205325.
[108] E. Scalise, M. Houssa, G. Pourtois, V. Afanas'ev, A. Stesmans, *Nano Res.* **2012**, *5*, 43 – 48.
[109] W. S. Yun, S. W. Han, S. C. Hong, I. G. Kim, J. D. Lee, *Phys. Rev. B* **2012**, *85*, 033305.
[110] S. Bhattacharyya, A. K. Singh, *Phys. Rev. B* **2012**, *86*, 075454.
[111] S. Dey, H. S. S. R. Matte, S. Shirodkar, U. V. Waghmare, C. N. R. Rao, *Chem. Asian J.* **2013**, *8*, 1780 – 1784.
[112] A. M. Panich, A. I. Shames, R. Rosentsveig, R. Tenne, *J. Phys. Condens. Matter* **2009**, *21*, 395301.
[113] P. Murugan, V. Kumar, Y. Kawazoe, N. Ota, *Phys. Rev. A* **2005**, *71*, 063203.
[114] J. Zhang, J. M. Soon, K. P. Loh, J. Yin, J. Ding, M. B. Sullivian, P. Wu, *Nano Lett.* **2007**, *7*, 2370.
[115] D. Li, C. Zhang, G. D, R. Zeng, S. Wang, Z. Guo, Z. Chenc, H. Liua, *J. Chin. Chem. Soc.* **2012**, *59*, 1196 – 1200.
[116] S. Tongay, S. S. Varnoosfaderani, B. R. Appleton, J. Wu, A. F. Hebard, *Appl. Phys. Lett.* **2012**, *101*, 123105 – 123104.
[117] S. Mathew, K. Gopinadhan, T. K. Chan, X. J. Yu, D. Zhan, L. Cao, A. Rusydi, M. B. H. Breese, S. Dhar, Z. X. Shen, T. Venkatesan, J. T. L. Thong, *Appl. Phys. Lett.* **2012**, *101*, 102103 – 102105.
[118] A. Vojvodic, B. Hinnemann, J. K. Nørskov, *Phys. Rev. B* **2009**, *80*, 125416.
[119] a) H. S. S. R. Matte, K. S. Subrahmanyam, C. N. R. Rao, *J. Phys. Chem. C* **2009**, *113*, 9982 – 9985; b) C. N. R. Rao, H. S. S. R. Matte, K. S. Subrahmanyam, U. Maitra, *Chem. Sci.* **2012**, *3*, 45 – 52.
[120] Y. Li, Z. Zhou, S. Zhang, Z. Chen, *J. Am. Chem. Soc.* **2008**, *130*, 16739 – 16744.
[121] G. L. Frey, R. Tenne, M. J. Matthews, M. S. Dresselhaus, G. Dresselhaus, *Phys. Rev. B* **1999**, *60*, 2883 – 2892.
[122] a) A. Sundaresan, C. N. R. Rao, *Nano Today* **2009**, *4*, 96 – 106; b) A. Sundaresan, C. N. R. Rao, *Solid State Commun.* **2009**, *149*, 1197 – 1200.
[123] K. Taniguchi, A. Matsumoto, H. Shimotani, H. Takagi, *Appl. Phys. Lett.* **2012**, *101*, 042603 – 042603.
[124] R. F. Frindt, *Phys. Rev. Lett.* **1972**, *28*, 299 – 301.
[125] D. H. Galvan, J.-H. Kim, M. B. Maple, M. Avalos-Borja, E. Adem, *Fullerene Sci. Technol.* **2000**, *8*, 143 – 151.
[126] a) R. Matte, C. N. R. Rao, Unpublished results; b) M. Nath, S. Kar, A. K. Raychaudhuri, C. N. R. Rao, *Chem. Phys. Lett.* **2003**, *368*, 690 – 695.
[127] E. Coronado, C. Martí-Gastaldo, E. Navarro-Moratalla, E. Burzurí, A. Camón, F. Luis, *Adv. Mater.* **2011**, *23*, 5021 – 5026.
[128] F. Schwierz, *Nat. Nanotechnol.* **2012**, *5*, 487 – 496.
[129] Ref. [2a].
[130] B. Radisavljevic, A. Radenovic, J. Brivio, V. Giacometti, A. Kis, *Nat. Nanotechnol.* **2011**, *6*, 147 – 150.
[131] D. J. Late, B. Liu, H. S. S. R. Matte, V. P. Dravid, C. N. R. Rao, *ACS Nano* **2012**, *6*, 5635 – 5641.
[132] H. Liu, P. D. Ye, *IEEE Electron Device Lett.* **2012**, *33*, 1273 – 1275.
[133] S.-W. Min, H. S. Lee, H. J. Choi, M. K. Park, T. Nam, H. Kim, S. Ryu, S. Im, *Nanoscale* **2013**, *5*, 548 – 551.
[134] Y. Zhang, J. Ye, Y. Matsuhashi, Y. Iwasa, *Nano Lett.* **2012**, *12*, 1136 – 1140.
[135] J. Pu, Y. Yomogida, K.-K. Liu, L.-J. Li, Y. Iwasa, T. Takenobu, *Nano Lett.* **2012**, *12*, 4013 – 4017.
[136] B. Chakraborty, A. Bera, D. V. S. Muthu, S. Bhowmick, U. V. Waghmare, A. K. Sood, *Phys. Rev. B* **2012**, *85*, 161403.
[137] K. Lee, H.-Y. Kim, M. Lotya, J. N. Coleman, G.-T. Kim, G. S. Duesberg, *Adv. Mater.* **2011**, *23*, 4178 – 4182.
[138] S. Ghatak, A. N. Pal, A. Ghosh, *ACS Nano* **2011**, *5*, 7707 – 7712.
[139] B. Radisavljevic, M. B. Whitwick, A. Kis, *Appl. Phys. Lett.* **2012**, *101*, 043103.
[140] H. Qiu, L. Pan, Z. Yao, J. Li, Y. Shi, X. Wang, *Appl. Phys. Lett.* **2012**, *100*, 123104.
[141] S. Das, H.-Y. Chen, A. V. Penumatcha, J. Appenzeller, *Nano Lett.* **2013**, *13*, 100 – 105.
[142] W. J. Yu, Z. Li, H. Zhou, Y. Chen, Y. Wang, Y. Huang, X. Duan, *Nat. Mater.* **2012**, DOI: 10.1038/nmat3518.
[143] W. S. Hwang, M. Remskar, R. Yan, V. Protasenko, K. Tahy, S. D. Chae, P. Zhao, A. Konar, H. G. Xing, A. Seabaugh, D. Jena, *Appl. Phys. Lett.* **2012**, *101*, 013107.
[144] S. Larentis, B. Fallahazad, E. Tutuc, *Appl. Phys. Lett.* **2012**, *101*, 223104.
[145] V. Podzorov, M. E. Gershenson, C. Kloc, R. Zeis, E. Bucher, *Appl. Phys. Lett.* **2004**, *84*, 3301 – 3303.
[146] H. Fang, S. Chuang, T. C. Chang, K. Takei, T. Takahashi, A. Javey, *Nano Lett.* **2012**, *12*, 3788 – 3792.
[147] a) L. Song, Z. Liu, A. L. M. Reddy, N. T. Narayanan, J. Taha-Tijerina, J. Peng, G. Gao, J. Lou, R. Vajtai, P. M. Ajayan, *Adv. Mater.* **2012**, *24*, 4878 – 4895; b) N. Kumar, K. Moses, K. Pramoda, S. N. S. Shirodkar, A. K. Mishra, U. V. Waghmare, A. Sundaresan, C. N. R. Rao, *J. Mater. Chem. A* **2013**, *1*, 5806 – 5821.
[148] K. Gopalakrishnan, K. Moses, a. A. Govindaraj, C. N. R. Rao, *Solid State Commun.* **2013**, DOI: 10.1016/j.ssc.2013.02.005.
[149] G. Cunningham, M. Lotya, N. McEvoy, G. S. Duesberg, P. van der Schoot, J. N. Coleman, *Nanoscale* **2012**, *4*, 6260 – 6264.
[150] L. Yang, S. Wang, J. Mao, J. Deng, Q. Gao, Y. Tang, O. G. Schmidt, *Adv. Mater.* **2012**, *25*, 1180 – 1184.
[151] J. Liu, Z. Zeng, X. Cao, G. Lu, L.-H. Wang, Q.-L. Fan, W. Huang, H. Zhang, *Small* **2012**, *8*, 3517 – 3522.
[152] K. Zhou, S. Jiang, C. Bao, L. Song, B. Wang, G. Tang, Y. Hu, Z. Gui, *RSC Adv.* **2012**, *2*, 11695 – 11703.
[153] R. R. Haering, J. A. R. Stiles, K. Brandt, (Ed.: US Patent 4224390), **1980**.
[154] G. Du, Z. Guo, S. Wang, R. Zeng, Z. Chen, H. Liu, *Chem. Commun.* **2010**, *46*, 1106 – 1108.
[155] C. Feng, J. Ma, H. Li, R. Zeng, Z. Guo, H. Liu, *Mater. Res. Bull.* **2009**, *44*, 1811 – 1815.
[156] S. Ding, D. Zhang, J. S. Chen, X. W. Lou, *Nanoscale* **2012**, *4*, 95 – 98.
[157] H. Li, W. Li, L. Ma, W. Chen, J. Wang, *J. Alloys Compd.* **2009**, *471*, 442 – 447.
[158] H. Hwang, H. Kim, J. Cho, *Nano Lett.* **2011**, *11*, 4826 – 4830.
[159] a) C. M. Julien, *Mater. Sci. Eng. R* **2003**, *40*, 47 – 102; b) B. Yebka, C. Julien, *Solid State Ionics* **1996**, *90*, 141 – 149.
[160] G. X. Wang, S. Bewlay, J. Yao, H. K. Liu, S. X. Dou, *Electrochem. Solid-State Lett.* **2004**, *7*, A321 – A323.
[161] S. Wang, G. Li, G. Du, L. Li, X. Jiang, C. Feng, Z. Guo, S. Kim, *Nanoscale Res. Lett.* **2010**, *5*, 1301 – 1306.
[162] C. Feng, L. Huang, Z. Guo, H. Liu, *Electrochem. Commun.* **2007**, *9*, 119 – 122.

[163] J.-w. Seo, Y.-w. Jun, S.-w. Park, H. Nah, T. Moon, B. Park, J.-G. Kim, Y. J. Kim, J. Cheon, *Angew. Chem.* **2007**, *119*, 8984 – 8987; *Angew. Chem. Int. Ed.* **2007**, *46*, 8828 – 8831.
[164] H. Liu, D. Su, G. Wang, S. Z. Qiao, *J. Mater. Chem.* **2012**, *22*, 17437 – 17440.
[165] R. Bhandavat, L. David, G. Singh, *J. Phys. Chem. Lett.* **2012**, *3*, 1523 – 1530.
[166] M. Winter, R. J. Brodd, *Chem. Rev.* **2004**, *104*, 4245 – 4270.
[167] A. Ghosh, K. S. Subrahmanyam, K. S. Krishna, S. Datta, A. Govindaraj, S. K. Pati, C. N. R. Rao, *J. Phys. Chem. C* **2008**, *112*, 15704 – 15707.
[168] K. Shiva, H. B. Rajendra, K. S. Subrahmanyam, A. J. Bhattacharyya, C. N. R. Rao, *Chem. Eur. J.* **2012**, *18*, 4489 – 4494.
[169] K. Chang, W. Chen, *Chem. Commun.* **2011**, *47*, 4252 – 4254.
[170] S. K. Das, R. Mallavajula, N. Jayaprakash, L. A. Archer, *J. Mater. Chem.* **2012**, *22*, 12988 – 12992.
[171] K. Chang, W. Chen, L. Ma, H. Li, H. Li, F. Huang, Z. Xu, Q. Zhang, J.-Y. Lee, *J. Mater. Chem.* **2011**, *21*, 6251 – 6257.
[172] K. Chang, W. Chen, *ACS Nano* **2011**, *5*, 4720 – 4728.
[173] K. Shiva, H. S. S. R. Matte, H. B. Rajendra, A. J. Bhattacharyya, C. N. R. Rao, *Nano Energy* **2013**, DOI: 10.1016/j.nanoen.2013.02.001.
[174] a) R. Prins in *Adv. Catal.*, *Vol. 46*, Academic Press, New York, **2001**, pp. 399 – 464; b) J. V. Lauritsen, M. Nyberg, J. K. Nørskov, B. S. Clausen, H. Topsøe, E. Lægsgaard, F. Besenbacher, *J. Catal.* **2004**, *224*, 94 – 106.
[175] F. Y. Cheng, J. Chen, X. L. Gou, *Adv. Mater.* **2006**, *18*, 2561 – 2564.
[176] Y. Tsverin, R. Popovitz-Biro, Y. Feldman, R. Tenne, M. R. Komarneni, Z. Yu, A. Chakradhar, A. Sand, U. Burghaus, *Mater. Res. Bull.* **2012**, *47*, 1653 – 1660.
[177] B. G. Rao, H. S. S. R. Matte, P. Chaturbedy, C. N. R. Rao, *ChemPlusChem* **2013**, *78*, 419 – 422.
[178] X. Zhong, H. Yang, S. Guo, S. Li, G. Gou, Z. Niu, Z. Dong, Y. Lei, J. Jin, R. Li, J. Ma, *J. Mater. Chem.* **2012**, *22*, 13925 – 13927.
[179] B. Hinnemann, P. G. Moses, J. Bonde, K. P. Jørgensen, J. H. Nielsen, S. Horch, I. Chorkendorff, J. K. Nørskov, *J. Am. Chem. Soc.* **2005**, *127*, 5308 – 5309.
[180] T. F. Jaramillo, K. P. Jørgensen, J. Bonde, J. H. Nielsen, S. Horch, I. Chorkendorff, *Science* **2007**, *317*, 100 – 102.
[181] C. Ataca, S. Ciraci, *Phys. Rev. B* **2012**, *85*, 195410.
[182] a) D. Merki, X. Hu, *Energy Environ. Sci.* **2011**, *4*, 3878 – 3888; b) A. B. Laursen, S. Kegnaes, S. Dahl, I. Chorkendorff, *Energy Environ. Sci.* **2012**, *5*, 5577 – 5591.
[183] D. Merki, S. Fierro, H. Vrubel, X. Hu, *Chem. Sci.* **2011**, *2*, 1262 – 1267.
[184] Z. Wu, B. Fang, A. Bonakdarpour, A. Sun, D. P. Wilkinson, D. Wang, *Appl. Catal. B* **2012**, *125*, 59 – 66.
[185] J. Kibsgaard, Z. Chen, B. N. Reinecke, T. F. Jaramillo, *Nat. Mater.* **2012**, *11*, 963 – 969.
[186] V. W.-h. Lau, A. F. Masters, A. M. Bond, T. Maschmeyer, *Chem. Eur. J.* **2012**, *18*, 8230 – 8239.
[187] Y. Li, H. Wang, L. Xie, Y. Liang, G. Hong, H. Dai, *J. Am. Chem. Soc.* **2011**, *133*, 7296 – 7299.
[188] E. G. S. Firmiano, M. A. L. Cordeiro, A. C. Rabelo, C. J. Dalmaschio, A. N. Pinheiro, E. C. Pereira, E. R. Leite, *Chem. Commun.* **2012**, *48*, 7687 – 7689.
[189] W. Zhou, Z. Yin, Y. Du, X. Huang, Z. Zeng, Z. Fan, H. Liu, J. Wang, H. Zhang, *Small* **2013**, *9*, 140 – 147.
[190] Q. Xiang, J. Yu, M. Jaroniec, *J. Am. Chem. Soc.* **2012**, *134*, 6575 – 6578.
[191] a) X. Zong, H. Yan, G. Wu, G. Ma, F. Wen, L. Wang, C. Li, *J. Am. Chem. Soc.* **2008**, *130*, 7176 – 7177; b) X. Zong, G. Wu, H. Yan, G. Ma, J. Shi, F. Wen, L. Wang, C. Li, *J. Phys. Chem. C* **2010**, *114*, 1963 – 1968.
[192] F. A. Frame, F. E. Osterloh, *J. Phys. Chem. C* **2010**, *114*, 10628 – 10633.
[193] P. D. Tran, S. S. Pramana, V. S. Kale, M. Nguyen, S. Y. Chiam, S. K. Batabyal, L. H. Wong, J. Barber, J. Loo, *Chem. Eur. J.* **2012**, *18*, 13994 – 13999.
[194] S. Min, G. Lu, *J. Phys. Chem. C* **2012**, *116*, 25415 – 25424.
[195] H. Li, Z. Yin, Q. He, H. Li, X. Huang, G. Lu, D. W. H. Fam, A. I. Y. Tok, Q. Zhang, H. Zhang, *Small* **2012**, *8*, 63 – 67.
[196] Q. He, Z. Zeng, Z. Yin, H. Li, S. Wu, X. Huang, H. Zhang, *Small* **2012**, *8*, 2994 – 2999.
[197] S. Wu, Z. Zeng, Q. He, Z. Wang, S. J. Wang, Y. Du, Z. Yin, X. Sun, W. Chen, H. Zhang, *Small* **2012**, *8*, 2264 – 2270.
[198] D. J. Late, Y. K. Huang, B. Lui, J. Luo, A. Yan, V. P. Dravid, C. N. R. Rao, Unpublished results.
[199] H. S. Lee, S.-W. Min, Y.-G. Chang, M. K. Park, T. Nam, H. Kim, J. H. Kim, S. Ryu, S. Im, *Nano Lett.* **2012**, *12*, 3695 – 3700.
[200] W. Choi, M. Y. Cho, A. Konar, J. H. Lee, G.-B. Cha, S. C. Hong, S. Kim, J. Kim, D. Jena, J. Joo, S. Kim, *Adv. Mater.* **2012**, *24*, 5832 – 5836.
[201] S. Bertolazzi, J. Brivio, A. Kis, *ACS Nano* **2011**, *5*, 9703 – 9709.
[202] A. Castellanos-Gomez, M. Poot, G. A. Steele, H. S. J. van der Zant, N. Agraït, G. Rubio-Bollinger, *Adv. Mater.* **2012**, *24*, 772 – 775.
[203] T. Li, *Phys. Rev. B* **2012**, *85*, 235407.
[204] M. S. R. N. Kiran, K. Raidongia, U. Ramamurty, C. N. R. Rao, *Scr. Mater.* **2011**, *64*, 592 – 595.